5. The Nature of Microphases in Ferritic Weld Metal Deposits

5.1 Introduction

Having discussed the phase transformation theory for the ferritic phases present in low alloy steel weld deposits, attention can now be turned to the 'microphases' associated with each of the prior formed phases. As mentioned previously, the volume fractions of Widmanstätten α and α_{acic} normally quoted also include the microphase between the plates and no attempt is usually made to determine which of the components - martensite, carbides or retained austenite are present and their relative abundances. The nature and extent of the various components in the microphase regions may have important consequences on fracture processes, e.g. large areas of martensitic plates can assist the propagation of cleavage cracks between α_{acic} plates or, more deleteriously, between Widmanstätten α plates. Thus the full benefit of an α_{acic} microstructure would not be experienced. The presence of carbides during ductile rupture can assist in nucleating secondary voids during growth and coalescence of the initial voids, which are more likely to form first on the much larger oxide inclusions present. Therefore, some prediction of the nature and distribution of the microphases is necessary for an accurate assessment of the properties of a weld.

5.2 Experimental

The same weld series (PJ303-306) was used as for the α_{acic} work in chapter 4 and the compositions were given in Table IV.1. In order to find the distribution of microphase components the variation of the martensite start temperature (M_S) with carbon content was calculated and is shown in fig 5.1. This carbon/M_S relation was obtained from a program devised to predict transformation time temperature (TTT) diagrams [81], which is used in the BSG model. The basis of this calculation is the balancing of the driving force for nucleation of martensite, $\Delta F_{Ms}^{\gamma-\alpha'}$, against the free energy change available from the austenite (γ) to martensite transformation.

$\Delta F_{Ms}^{\gamma-\alpha'}$ is calculated on the basis of the thermodynamic formalisms of Lacher [181] and Fowler and Guggenheim [182], (LFG). This approach [183] accounts well for the stored energy of a martensite plate and predicts values of $\Delta F_{Ms}^{\gamma-\alpha'}$ between -900 and -1400Jmol^{-1}. The values of $\Delta F_{Ms}^{\gamma-\alpha'}$ vary with carbon content, but neither monotonically nor to a great extent. A plot of $\Delta F_{Ms}^{\gamma-\alpha'}$ vs. carbon content exhibits a minimum due to Zener ordering, at higher [C], reducing the free energy of martensite relative to austenite.

The available free energy change from the γ-martensite transformation is determined by an extrapolation of the γ and α free energy surfaces to temperatures, where the two phases are not

in thermodynamic equilibrium. These regimes can be covered by modifications [184-186] of the LFG approach and can incorporate some account of the effects of substitutional alloying elements. These are incorporated by the changes introduced into both the magnetic and non-magnetic free energy components of the γ-α transformation in pure iron. A second effect, not as accurately modelled as that just mentioned, is the C-Y (Y=substitutional alloying element) interaction, which is dealt with by a modification of the C-C pairwise interaction energy. This is essentially a 'superelement' approach, where the substitutional lattice is replaced by an array of averaged, hypothetical atoms, ignoring the separate character of Fe and Y. This introduces some approximations, but gives reasonable agreement, at least within the equilibrium regime.

Another approximation arises from the assumption that $\Delta F_{Ms}^{\gamma-\alpha'}$ is a function only of carbon content, i.e. the values for Fe-C and Fe-C-Y are identical. As carbon is expected to exert the largest effect on martensite crystallography and substructure, but even this is a small effect, then the approximation is valid in low alloy cases.

Use of this analysis gives M_s temperatures, that agree to within 10-20°C of experimental values [187].

Fig 5.1 indicates that M_s is reduced to ambient temperatures for austenite containing carbon mole fractions of:

0.033	PJ303	Fe-0.121 C-3.09 Mn-0.41 Si
0.040	PJ305	Fe-0.180 C-1.40 Mn-1.52 Si
0.038	PJ304/PJ306	Fe-0.201 C-1.80 Mn-0.44 Si

Hence, any region of austenite, in a volume of microphase, enriched to or above these levels by carbon partition into it from the various ferrite phases, will be retained to room temperature. Therefore, the extent of retained austenite (γ_r) can be used as a rough indicator of regions of carbon levels greater than those above, for each composition. The kinetics of martensitic transformations are generally so rapid that they do not need to be considered so that prediction of the martensite/retained austenite regime can be covered by a thermodynamic approach. That is, if it is thermodynamically possible to form martensite in a region of microphase, then it will form, when that favourable condition is attained. The formation of carbides, however, may be subject to kinetic constraints. At high transformation temperatures the transformation products will be largely diffusional in character so that any carbides expected would be a type of degenerate pearlite, whose formation is subject to the kinetic control inherent in the nucleation and growth of alternate α/Fe_3C plates. The kinetics of pearlite formation are generally slow compared to the cooling times typical of welding processes, although in high heat input processes, such as submerged arc (SA) welding, slower cooling rates would allow the development of some small scale pearlitic regions.

Lower transformation temperatures, and lower heat input processes lead to a preponderance of displacive products (Widmanstätten α, α_{acic} and α_b) over diffusional and a change in the nature of any carbides, which will become much finer, adopting a rational orientation relationship with

the parent phase and will be similar to the carbides found in lower bainite or autotempered martensite.

The interrelationships between ferritic phases and microphases were studied using a series of isothermal heat treatments to vary the proportions of the ferritic phases present in the samples. These heat treatments were carried out, for convenience, in a Theta Industries high speed dilatometer. The facilities of a low thermal mass radio frequency (RF) heating coil and helium quenching give very rapid responses to temperature changes and so minimise any transformations whilst reaching the isothermal treatment temperature after reaustenitisation.

A knowledge of the transformation mechanisms operative in the formation of Widmanstätten α and α_{acic} allows the carbon level in the austenite remaining when ferrite formation ceases to be calculated as a function of temperature. Widmanstätten α, which forms with interfacial equilibrium maintained with respect to carbon, will proceed to the paraequilibrium volume fraction, i.e. until the carbon level of the remaining austenite reaches the Ae_3' value at that temperature, fig 2.36. The absence of any substitutional diffusion during the formation of Widmanstätten α means that the paraequilibrium limit applies rather than the full equilibrium Ae_3, which requires partition of the substitutional alloying elements between α and γ. Acicular ferrite, being a form of bainite, forms with a full supersaturation of carbon by a displacive mechanism. Hence, formation of α_{acic} will cease when α and γ of the same composition (initially the bulk composition of the sample) have the same free energy, so that the driving force for lattice transformation is reduced to zero, fig 2.36. This defines the T_0 composition at this temperature. The shear component of the lattice transformation gives rise to a strain energy term, which opposes the reaction and so the formation of α_{acic} stops before T_0 is reached, at T_0'which is the carbon level of the remaining γ when the driving force for transformation just equals the strain energy involved, fig 2.36.

Table V.1 lists the heat treatments used, which were chosen so that full transformation should give retained austenite for Widmanstätten α and/or α_{acic}. This was achieved by the use of isothermal temperatures of 500-520°C. In addition the formation of pearlite was investigated by use of higher ($\approx$ 680°C) transformation treatments. The specimens were reaustenitised, prior to isothermal treatment, at 1000 or 1200°C for 10 minutes and helium quenched to the isothermal treatment temperature. The entire heat treatment, being carried out in the Theta Industries high speed dilatometer.

The specimens were prepared as 3mm diameter rods, 15mm in length machined parallel to the welding direction and nickel plated (see chapter 3 for details) to reduce surface nucleation of ferrite. After heat treatment and final quenching to room temperature the rods were slit under flood lubrication to discs before thinning to 0.05mm and jet polishing in a 95% acetic acid- 5% perchloric acid electrolyte at 20-80V and room temperature. The foils were examined in a Philips 400T TEM operating at 120kV and fitted with a Link series 860 EDS attachment. EDS analysis was performed to determine the substitutional alloying element content in specific microphase

regions so that a more accurate estimation of the local thermodynamics. Use of selected area diffraction patterns (SADP), bright and dark field images then permitted identification of the phases constituting the microphase regions under different conditions.

5.3 Overall Microstructure

5.3.1 680°C Treatments

This temperature corresponds to the upper portion of the ferrite transformation range and the phase formed is grain boundary nucleated allotriomorphic ferrite, which develops with unequal matching with the adjacent γ grains. This results in more rapid growth of the allotriomorphs into the γ grain with which they have a lower energy interface compared with the other grain, fig 5.2. Incomplete homogenisation, probably resulting from long range segregation in the weld, causes a variation in the volume fraction of ferrite (V_α) formed through the specimen, fig 5.3, but the effects upon the microphase regions were entirely consistent once this variation was taken into account. The very rapid cooling, allied with the relatively high alloying contents, meant that the majority of the microphases were martensitic. At very short transformation times, when V_α is small, then bainite sheaves are evident emanating from α/γ interfaces, fig 5.4, either as a single sheaf or as a packet, fig 5.5. The transformation temperature is well above that at which bainite formation is thermodynamically possible and so these sheaves must have formed rapidly during the quench to room temperature. Fig. 5.6 illustrates the effect that variation of the isothermal holding time at 680°C has upon the volume fraction of allotriomorphic α and the associated microphases.

Relatively short isothermal times (t_{iso}), 30 minutes, give a small amount of allotriomorphic ferrite (15-20%) decorating the prior austenite grain boundaries. The associated microphases consist of martensite with substantial amounts of bainite and some Widmanstätten α. At increased isothermal times, 60 minutes, the volume fraction of allotriomorphic α increases to 34-38% resulting in greater partition of carbon into the remaining γ. The subsequent increase in hardenability of this region, due to higher C levels, causes a decrease in the proportions of Widmanstätten α and bainite, fig. 5.6b. Eventually, Widmanstätten α (first) and bainite are eliminated to leave martensite as the sole microphase constituent at higher volume fractions ($\approx$ 40%) of ferrite. Further increases in t_{iso} results in sufficient carbon partition, from increased allotriomorphic α formation, and time to nucleate carbides, leading to the presence of pearlite in the microphase. The longest isothermal holding time (20.5 hours) gives a fully pearlitic microphase, fig. 5.6e. The formation of pearlite takes place too rapidly at these carbon levels to allow the formation of allotriomorphic α to cause austenite retention down to room temperature. Specimen PJ306 HC, 5.28 hours at 680°C, fig 5.7, has a large V_α ($\approx$ 50%) and exhibits microphase regions of pearlite and martensite in quite distinct areas. EDS analysis reveals no great difference in substitutional alloying element content between regions of pearlite and those of martensite, Table V.2. In addition the values of V_α surrounding either type of microphase were

similar so that the partitioned carbon levels should be similar. Therefore other factors must favour the nucleation of pearlite in these grains, which then rapidly grows to completely transform that region to pearlite. In grains where nucleation does not take place then the microphase region remains austenitic until M_s is reached. The use of a highly extended heat treatment, PJ306 HB, 20.5 hours at 680°C, results in complete transformation to a pearlitic structure, fig 5.8. This is clearly improbable in a welding cycle, but does illustrate the great role that carbon partition from the ferritic phases has upon later transformations. The values of V_α were used to calculate the carbon level in the remaining austenite, x_c^γ, (table V.3) from the equilibrium carbon level in the ferrite, x_c^α, and the bulk carbon level, x_c^o, using the equation:

$$x_c^\gamma=(x_c^o-V_\alpha x_c^\alpha)/(1-V_\alpha) \qquad .....(42)$$

This value can then be used to calculate the TTT curve for the enriched austenite to determine the expected transformation behaviour of the untransformed γ. Analysis of these plots, along with the corresponding T_o, T_o' and Ae_3 curves shows that it is the hardenability effect that is responsible for the change in microphase.

Therefore, for allotriomorphic ferrite, the effects of transformation can be dealt with through the TTT curve and its conversion into a CCT curve.

5.3.2 500-520°C

This temperature regime offers great possibilities for microphase study as the rate of transformation for diffusional products is low giving a microstructure dominated by Widmanstätten α, α_{acic} and microphases. Additionally, if both the ferritic phases proceed to their maximum extent then carbon partition from Widmanstätten α should stabilise γ down to room temperature, but the much smaller partition from α_{acic} would not be expected to do so. Therefore α_{acic} would be associated with martensite if carbon partitioned uniformly through the remaining austenite. The isothermal treatment temperature is just below the bay in the TTT diagram, fig 5.9, and so both types of ferrite are to be expected in the same specimen allowing direct comparison of the two. A disadvantage of this temperature is that it is very sensitive to variations in the substitutional alloying element levels. This can result in a variation in the ferrite phase that is inconsistent with the heat treatment time variations. This would be due to variations in the substitutional alloying element contents between specimens and between different regions of the same specimen, as has already been noted. This was seen the series of specimens at both temperatures used and was a consequence of long range segregation in the weld. The use of locally reported EDS data helped to counter this effect.

Optically, the microstructure consisted of a series of lath structures Widmanstätten α, α_{acic} and bainite to various extents with attendant microphase regions composed of several phases.

The use of very short isothermal treatment times gives a microstructure consisting of grain boundary and intragranularly nucleated bainite sheaves, fig 5.10. The former sheaves are present as colonies of parallel plates, whereas the latter are non-parallel 'star' formations. The presence of

a small amount of Widmanstätten α is also noted. The very short times are insufficient for Widmanstätten α nucleation at the prior γ grain boundaries and so this corresponds to a continuous quench with bainite forming over a range of temperatures. It is not possible to determine which has formed first, grain boundary or intragranular bainite, but the intragranular sheaves have developed to a large size, much coarser than typical α_{acic} plates. This may be due to the lack of significant carbon partition and the absence of other ferrite phases with which it might impinge. Extension of the treatment time has two effects, fig 5.11:

(i) the intragranular plates become more refined than the bainite above and are more characteristic of α_{acic} structures.

(ii) Widmanstätten α is seen to be nucleated at the prior γ grain boundaries.

The microphases in these specimens consist of a grey etching phase and one that etches much more darkly; these could not be identified optically. The microstructure resulting from much longer isothermal times, fig 5.12, is composed entirely of lath products with the prior γ grain boundaries etching very darkly. The series of isothermal runs performed on PJ303 specimens gave similar trends, although the shortest time used in this case was 30 minutes, resulting in well developed Widmanstätten α and α_{acic} colonies, fig 5.13. A dark etching phase was again observed to form at prior γ grain boundaries with extended isothermal times.

The slightly higher temperature used, 520°C, and different alloy system, PJ306, gives rise to a microstructure dominated by α_{acic} with small amounts of allotriomorphic and Widmanstätten α, fig. 5.14. The transformations are extremely rapid and are largely completed after $\approx$ 300s so the effects of long holding times were not studied. Earlier studies of the long term stability of bainite have indicated interface instability with the initially smoothly curved α_b/γ interface becoming variegated. This is due to the very slow formation of ferrite, which shows no diffusion of substitutional alloying elements and maintains the crystallographic relationships of the original bainite [188].

5.4 Transmission Electron Microscope Studies

The detailed nature of the microphases could not be deduced using optical techniques and so transmission electron microscopy (TEM) was used to further monitor the variation in microphase type.

5.4.1 680°C Treatments

The shortest isothermal time (1800s) gave a microstructure of allotriomorphic α with microphases composed mostly of lath martensite and bainite. There were some examples of larger Widmanstätten α and bainite plates, fig. 5.15, within the matrix of martensite. Colonies of parallel α_b plates were seen separated by highly dislocated lath martensite, fig. 5.16, which contained some fine carbides (Fe_3C) when the spacing was small. As the interplate spacing was increased then evidence of twin martensite and retained austenite, as a thin rim around the

α_b/martensite interface, was seen, fig. 5.17. This variation of microphase with distance suggests there is unequal distribution of carbon away from the α_b/γ interface during post-shear partition. As V_α increases with extended isothermal treatment time greater partition of carbon into the remaining γ takes place and is associated with a decrease in the amount of Widmanstätten α observed. After 3600s (V_α=0.34-0.38) Widmanstätten α is almost completely absent and the microphases are dominated by bainite sheaves and martensite. The high M_s of these samples ($\approx$ 400°C) causes autotempering of the martensite, fig. 5.18, with precipitation of Fe_3C in some microphase regions. Increases in V_α were expected once the isothermal treatment time was extended to 10800s, but variations in overall alloying levels caused it to decrease to 0.230. This specimen displayed a wide range of transformation products subsequent to allotriomorphic ferrite, including secondary Widmanstätten α plates with interplate retained γ, α_b in star formations and autotempered martensite, fig. 5.19. The interplate γ associated with Widmanstätten α appears to be striated, which is more typical of twinned martensite, fig. 5.20, but this may be an artefact of the foil preparation as the ferrite also seems mottled indicating some etching. Adjacent to some of the allotriomorphs sufficient time has elapsed for the formation of some degenerate pearlite to take place, fig. 5.21. This process is repeated at 19008s by the formation of pearlite colonies between ferrite allotriomorphs with the elimination of both Widmanstätten α and bainite from the microphases, which are predominantly twinned martensite, fig 5.22. After very long holding at 680°C, 73800s, the microstructure contained just allotriomorphic ferrite and pearlite, which contained blocky carbides (Fe_3C). In addition the carbides were associated with dislocation cells and interface ledges/dislocations, fig. 5.23, similar to those reported by Shiflet [189].

5.4.2 500-520°C Treatments

The use of lower isothermal treatment temperatures gives rise to microstructures consisting mainly of displacive products such as Widmanstätten α, α_b and α_{acic}. This causes a reduction in the scale of the microphase regions, which are restricted to 'pockets' of more limited extent than the prior γ grain centres associated with grain boundary allotriomorphic ferrite. The presence of both Widmanstätten α and α_{acic} allows direct comparison of the microphase associated with each phase. The variation of microphases will now be considered for these two ferritic phases as the degree of transformation increases.

At low degrees of transformation, small packets of Widmanstätten α occur, whose laths are separated by martensite, which is predominantly of the twinned form, fig. 5.24. The microphases associated with Widmanstätten α were invariably of one type throughout the interplate region, which indicates a reasonably uniform carbon level in that region. In contrast, short isothermal times that develop α_{acic} lead to a very non-uniform distribution of microphases, fig. 5.25. Immediately adjacent to the α_{acic}/microphase interface, a thin layer of retained austenite is observed, which rapidly changes to martensite. Martensite comprises the bulk of the microphase and is predominantly of the lath (low carbon) type. Evidence of twinned martensite between γ_r and lath martensite was not readily seen. If uniformly distributed throughout the microphase

region, the partitioned carbon would not be expected to stabilise γ down to room temperature, but the Ae_3' carbon level would. It would, therefore, appear that, at short isothermal times, the interface achieves paraequilibrium with respect to carbon after shear formation of the ferrite. There is little time for carbon diffusion into the microphase and so the carbon level rapidly falls to the bulk concentration away from the α_{acic}/microphase interface.

On increasing the isothermal treatment time, two effects occur:

(i) There is increased opportunity for γ-α transformation, which is manifested in increasing volume fraction of Widmanstätten α and α_{acic}, with reduced microphase thicknesses between them.

(ii) Diffusion processes have more time in which to operate and so composition profiles become flatter and interface compositions deviate more from the Ae_3' values.

These transformation regimes see a change in the nature of microphases associated with Widmanstätten α from martensite to retained austenite, fig. 5.26. The changes noted in the microphases associated with α_{acic} depend more strongly on time and composition. Small increases in t_{iso} cause the layer of γ_r to increase in thickness and the appearance of twinned martensite between that and the central lath martensite, fig. 5.27. Further increases in t_{iso} cause increased thicknesses of both retained austenite and twinned martensite at the expense of lath martensite, fig. 5.28. Eventually, however, the retained austenite disappears, to be replaced by twinned martensite, which go on to dominate the microphase region, fig. 5.29.

This behaviour can be rationalised by considering the increased diffusion of carbon away from the α_{acic}/microphase interface. At very short times, little diffusion of C into the microphase occurs, as there is only a small amount to redistribute and little time available. However, if diffusion can take place, then the microphase further from the interface with α_{acic} will be enriched to a greater extent forming more twinned martensite and retained austenite. The finite amount of C available means that the redistribution will decrease the interfacial concentration and flatten the profile away from the interface. Therefore, when the carbon profile is flattened out and reduced, so that it falls below the value required to retain γ, the γ_r will disappear with the microphase forming (high carbon) twinned martensite instead.

During these heat treatments Widmanstätten α is still associated with γ_r but, as t_{iso} is increased, the incubation time for carbide nucleation is exceeded and these are precipitated at the γ/Widmanstätten α interface, in γ, fig. 5.30. The long times at $\approx$ 500°C needed to replace γ_r by twinned martensite around α_{acic}, 3 hours, cause complete carbide precipitation between Widmanstätten α plates to give α and Fe_3C.

These changes are indicative of different levels of carbon partition into the unreacted austenite with the carbon level decreasing in the order:

Carbides>γ_r>twin martensite>lath martensite

EDS microanalysis, carried out in a Philips 400T TEM, showed no variation in substitutional alloying element levels between the different microphase regions or indeed between the displacive

ferrite products and the adjacent microphase, fig. 4.28.

This sequence of events was repeated when a multistep approach was adopted. In these specimens the reaustenitisation treatment (10 minutes at 1000 or 1200°C) was followed by isothermal treatments at

(i) 680°C, then

(ii) 500-520°C

the object of this being to vary the amount of allotriomorphic α formed and so change the overall carbon level of the austenite from which Widmanstätten α and α_{acic} form. Increase in the carbon level had the same effect as increasing the isothermal treatment for the original single step treatment. The microphase constituents change along the series

lath α' then twin α' then γ_r then carbides

Again lath martensite is rarely associated with Widmanstätten α and carbides not often seen in interplate regions for α_{acic}.

A consideration of the transformation mechanisms operating during and after formation of each phase can be used to model this behaviour. The major difference between these phases is the extent of carbon diffusion during formation of the ferrite phase. Widmanstätten α is a carbon diffusion controlled transformation and maintains equilibrium at the interface with respect to carbon. Redistribution of carbon therefore takes place rapidly and the carbon level of the residual austenite can rise to the equilibrium value defined by the Ae_3' curve. As Widmanstätten α is a displacive product, there is no partition of substitutional alloying elements during its formation and so equilibrium is subject to the constraint of equal concentrations of substitutional alloying elements in both phases. Hence the use of the Ae_3' curve rather than Ae_3. Redistribution of carbon in the residual austenite to a uniform concentration after ferrite formation is determined only by the rate of diffusion of carbon in the enriched γ. Carbon profiles during and after Widmanstätten α formation are shown in fig. 5.31.

Acicular ferrite, being a form of bainite, forms by a fully displacive mechanism and so inherits a full supersaturation of carbon from the parent austenite. After formation of a ferrite sub-unit carbon partition into the remaining austenite takes place, which will be governed by two processes:

(i) Carbon will take a finite time to diffuse out of the ferrite sub-unit, subject to interface equilibrium with respect to carbon.

(ii) Redistribution of carbon in austenite will take place, once the ferrite is denuded in carbon. This process will be the same as for Widmanstätten α, but at generally lower carbon levels.

Of these (i) will be faster as carbon diffusion in ferrite is more rapid than that in austenite. The level of carbon partition into austenite is less than for Widmanstätten α as once γ is enriched in carbon to the level defined by the T_0 or T_0' curves the driving force for diffusionless reactions is reduced to zero and no further ferrite formation is possible. Fig. 5.32 illustrates the carbon profile during and after α_{acic} formation.

Therefore, in determining the carbon level in γ at the formation of the various microphase components, several factors are important:

(i) The extent of carbon diffusion during formation of the ferrite phase and its volume fraction.

(ii) The rate of carbon redistribution from that phase.

(iii) The extent of the microphase region in which redistribution occurs.

These will determine the carbon level in the residual austenite as a function of time, temperature and distance from the ferrite phase and so the nature of the final decomposition products.

In respect to point (iii) above, it is necessary to consider the geometries adopted by the microphase regions in relation to the associated ferrite phases. The results of TEM studies could be broadly classified into three types of geometry and these are shown in fig 5.33, along with their important dimensions. Table V.3 summarises the results obtained from the TEM images of the dimensions of each microphase constituent for different heat treatments. This indicates a strong dependence of the thickness of each component upon the ratio of microphase width to ferrite width, i.e. upon the amount of carbon being redistributed and the distances it has to diffuse.

5.4.2.1 Widmanstätten Ferrite

The colonies of Widmanstätten α exhibited a series of parallel plates, whose spacing was generally less than the plate width (typically spacing=0.01-0.50 of the width). The α/microphase interface was straight over a large portion of its length so that the width and spacing remained approximately constant. The interplate microphase was generally of one type, either retained austenite or twin α'. The overall planar and parallel nature of this phase mean that the redistribution of carbon away from the interface can be considered as a one-dimensional process normal to the interface between ferrite and the microphases.

5.4.2.2 Acicular Ferrite

This phase shows a much wider range of microphases with the width of the microphase region generally 2-3 times that of the ferrite, hence carbon enrichment would be expected to be much less than for Widmanstätten α. However, the layers of each microphase component are parallel to the original α_{acic}/γ interface, which displays a large degree of planarity. Therefore, it appears that the redistribution of carbon is again unidirectional, normal to the interface and can be modelled by the one dimensional diffusion of carbon away from the interface.

5.5 Modelling Carbon Redistribution

This is probably easier to apply to α_{acic} initially. Referring back to fig 5.33 the carbon profile during ferrite formation is uniform throughout both phases, so it can be assumed that the starting conditions are a uniform carbon concentration, which persists until the ferritic unit has

formed. After ferrite formation, equilibrium is attained at the interface whilst carbon is partitioned from ferrite to austenite.

If the microphase region is treated as a permeable membrane, then the attainment of equilibrium at the γ/α_{acic} interface is equivalent to the imposition of equal, constant surface compositions. Under these conditions the concentration C_x at a distance x from the interface is given by [190-194]:

$$C_x=C_0+(C_1-C_0)\left[1-\frac{4}{\pi}\sum_{n=0}^{\infty}\frac{(-1)^n}{(2n+1)}\exp\{-D(2n+1)^2\pi^2 t\}\cos\frac{(2n+1)\pi x}{2L}\right] \quad .....(43)$$

L=total width of microphase

C_1=surface concentration of carbon

C_0=initial concentration of carbon

As carbon diffuses at different rates in α and γ the rate at which partition from ferrite to austenite takes place is determined by the slower diffusion rate, i.e. that in γ. Equation 42 applies to both α and γ, but, in order to conserve mass across the interface, the following constraint applies.

$$D_\alpha\frac{\partial C_\alpha}{\partial x}=D_\gamma\frac{\partial C_\gamma}{\partial x} \quad .....(44)$$

at the interface.

In addition the interface concentrations are constant at the equilibrium values.

The carbon profile is predicted initially by calculating the equilibrium carbon concentrations, which are the paraequilibrium values as the concentration of substitutional alloying elements across is constant across the interface. Equilibrium is calculated on the basis of Wagner interaction parameters. As D_γ is less than D_α, then the former will control the rate of carbon transfer across the interface. Hence, in order to solve equation 43, D_γ is first calculated using the equation [195,196]: $D_\gamma = 0.5\exp(-30C_\gamma)\exp[(140250 - 7.95\times10^5 C_\gamma + 2.3\times10^6 C_\gamma^2)/RT]$ cm^2s^{-1} for the equilibrium (interface) concentration of carbon.

Differentiation of equation 43 for α and γ gives the concentration gradients at the interface in α and γ as a function of D_α, D_γ and time. From the initial value of D_γ, equation 43 can be solved for D_α and the interfacial concentration gradients. This process is repeated at intervals of 0.01s during the decarburisation of the ferrite plate until the ferrite is fully decarburised. The concentration dependence of D_α is neglected as the value of this will be controlled by the interface constraint, equation 2. Utilising these values the carbon profiles in both ferrite and austenite are calculated at 0.01s intervals up to t_0, which is the time taken to fully decarburise ferrite. Full decarburisation is taken as the time for the carbon level at the centre of the ferrite plate to fall to C_0+0.00001. This analysis calculates the minimum time for decarburisation as the maximum values of D_α and D_γ, i.e. those obtaining at the interface, are used throughout the ferrite and austenite. The resulting carbon profile is illustrated in fig. 5.34 and decarburisation

times vary between 0.02 and 0.17 seconds dependent upon the relative dimensions of ferrite and microphases. These values can be compared with those proposed by Aaronson [186], which are much shorter around 0.003 seconds, but arise from the use of invalid assumptions in his calculation. Aaronson assumed that decarburisation of ferrite was achieved at the maximum rate in ferrite and neglected the necessity for C diffusion away from the interface in γ.

Equation 42 applies until the ferrite has been depleted in carbon, after which interface equilibrium will not be maintained as carbon which diffuses away from the interface into γ is not replaced from carbon exitting the ferrite. Still considering the microphase as a membrane, the interfaces now act as impermeable surfaces not permitting the diffusion of carbon into or out of the microphase. An analytical solution for this situation exists, derived by Crank and Henry [197], for a membrane whose surfaces are maintained at a constant concentration, C_1, for a time t_0 and then rendered impermeable. If f(x) is the initial concentration profile, as determined from equation 43, then $C_{x,t}$ is given by:

$$C_{x,t}=\frac{1}{2}\int_0^L f(x')dx' + \frac{2}{L}\sum_{n=0}^{\infty} \exp(-Dn^2\pi^2t/L^2) \times \cos\frac{n\pi x}{L}\int_0^L f(x')\cos\frac{n\pi x'}{L}dx' \quad .....(45)$$

where

$$f(x)=C_1\left[1-\frac{4}{\pi}\sum_{m=0}^{\infty}\frac{1}{2m+1}\sin\frac{(2m+1)x}{L}\exp(-D(2m+1)^2\pi^2t_0/L^2)\right] \quad .....(46)$$

L=total width of membrane (microphase)

and

$$\int_0^L f(x)dx=C_1L\left[1-\frac{8}{L}\sum_{m=0}^{\infty}\frac{1}{(2m+1)^2}\exp\frac{(-D(2m+1)^2\pi^2t_0)}{L^2}\right] \quad .....(47)$$

$$\int_0^L f(x)\cos\frac{2p\pi x}{L}dx=\frac{8C_1L}{\pi^2}\sum_{m=0}^{\infty}\frac{1}{4p^2+(2m+1)^2}\exp\frac{\{-D(2m+1)^2\pi^2t_0\}}{L^2} \quad .....(48)$$

A typical result for this analysis is shown in fig. 5.34 for carbon distributions for α_{acic} after heat treatment. Plots such as these were used to deduce the distance into the microphase at which sufficient carbon enrichment had occurred to retain γ to room temperature. This was done for the profile existing both immediately after decarburisation and that at the end of the heat treatment. These can be compared with the experimental values of retained austenite width measured from the TEM studies, bearing in mind that the TEM values might exceed the true width of γ_r normal to the interface as the interface normal may be at an angle to the plane of the TEM image. The comparison is presented in fig 5.35.

The case for Widmanstätten α differs in that carbon diffusion occurs during formation of the ferrite phase and is associated with point diffusion from the tip rather than from the flat surfaces. However, for this study, the same analysis was applied, which makes the assumption that the ferrite develops to its full width immediately and then redistributes carbon into austenite: this

assumption is reasonably valid as redistribution of carbon from α during growth is rapid and the rate determining step is homogenisation in γ. It is not possible to determine when each colony of Widmanstätten α plates formed and so over what time during the heat treatment carbon redistribution has taken place. Hence, as a comparison between the behaviour of α_{acic} and Widmanstätten α with respect to microphase formation, it is a valid analysis. A corresponding profile for Widmanstätten α is presented in fig. 5.36, and comparison with experimental results in fig. 5.37.

The comparisons reveal good agreement for the prediction of microphase nature for Widmanstätten α, but less agreement for α_{acic}. In the latter case, the agreement was better at t_0 than at the end of the heat treatment, suggesting that redistribution is less rapid than the model predicts. The analysis did not take account of the concentration dependence of diffusivity, the weighted average diffusivity of carbon in austenite being used for the second stage of the redistribution program. The effect of this is unlikely to be great with a greater effect arising from the deviation from equilibrium at the interface as carbon diffuses into the austenite. Deviations from equilibrium at the interface cause the activity of carbon to be increased so reducing the driving force for redistribution of carbon. Hence, the redistribution will take place more slowly than predicted by equation 45, as this does not take account of the activity of carbon and its effect upon diffusion, which takes place down an activity gradient.

A more accurate assessment of the carbon profile could be obtained by the use of an analytical or finite difference approach taking account of carbon activity.

5.6 Conclusions

The nature of microphase constituents has been found to be strongly dependent upon the extent of carbon redistribution from the prior formed ferritic phases. The weld metal chemistry and temperature at cessation of α_{acic} formation are also important, in that if the carbon level corresponding to Ae_3' at that temperature is high enough to retain γto room temperature, then a γ_r rim around α_{acic} is likely. This will form despite the carbon level for T_0 (or T_0') being too low to retain γ, if a non-uniform carbon distribution exists and the deviation from paraequilibrium at the interface is not too great. Prediction of microphases can, therefore, be achieved by modelling the carbon redistribution from those ferrite phases. This covers the formation of phases such as martensite/retained austenite, but a consideration of degenerate pearlite and carbides will require knowledge of the kinetics of carbide nucleation and growth.

These results are for isothermal treatments and must be converted to continuous cooling for application to welding processes. Widmanstätten α is assumed (BSG model) to form in the weld during cooling from the bay in the TTT curve to a temperature/time when impingement with α_{acic} occurs. The latter temperature is the one at which growth finishes and, if the width and spacing of the plates can be predicted, the amount of carbon redistribution during and after ferrite formation can be assessed. Thus microphase prediction for this phase is possible.

Acicular ferrite will form during the remaining cooling to room temperature (or interpass temperature for multipass welding). At each temperature the maximum amount of α_{acic} that can form is determined by the T_0 and T_0' curves. The early sub-units to form, i.e. those at higher temperatures, redistribute carbon uniformly through the remaining γ before subsequent sub-unit formation. As cooling continues, redistribution is incomplete so that subsequent sub-units form away from the carbon enriched interface. The interface region generally has carbon levels in excess of those corresponding to the T_0 or T_0' curves. Incomplete partition of carbon from ferrite at lower temperatures leads to supersaturated ferrite and a more 'spiked' interface carbon profile in austenite as less carbon has entered, but equilibrium must be maintained. Acicular ferrite formation and carbon partition will continue until the temperature of the least enriched region of microphases falls below M_s for that local composition. Once martensite formation has taken place carbon can no longer partition into that region. Further formation of α_{acic} is unlikely and the remaining transformations are extension of the martensite as temperature decreases or retention of austenite if regions are suitably enriched. Some carbon will redistribute throughout the remaining γ between the initial formation of martensite and room temperature, which will affect the amount of γ ultimately retained. This is summarised in fig. 5.38.

Table V.1. Heat treatments for microphases work.

Weld	Specimen	Reaustenitisation		Isothermal	
		Temp.(°C)	Time(s)	Temp.(°C)	Time(s)
PJ303	HA	1000	600	450	3010
	HB	1000	600	500	21100
	HC	1000	600	520	60200
	HD	1000	600	500	3600
	HE	1000	600	500	7200
	HF	1000	600	500	1800
PJ305	HA	1000	600	500	43200
	HB	1000	600	500	80
	HC	1000	600	500	317
	HD	1000	600	500	4068
	HE	1000	600	500	5
PJ306	HA	1000	600	680	10800
	HB	1000	600	680	73800
	HC	1000	600	680	19008
	HD	1000	600	680	3600
	HE	1000	600	680	1800
	HF	1000	600	680	43200
	SA	1200	600	502	300
	SB	1200	600	500	60
	SC	1200	600	500	20
	SD	1200	600	518	10
	SE	1200	600	520	4

Table V.2. EDS results for PJ306 HC, 1000°C/10 mins-680°C/19008s.

Region	Mn	Si	Cr
Pearlite	1·648	0·651	0·136
	1·734	0·526	0·126
	1·577	0·656	0·087
	1·506	0·409	0·037
	1·704	0·638	0·064
Martensite	1·696	1·033	0·114
	1·645	0·796	0·077
	1·149	0·721	0·157
	1·547	0·907	0·193
	1·863	1·067	0·033
Ferrite	1·824	0·940	0·125
	2·154	0·949	0·097
	1·620	0·570	0·174
	1·368	0·881	0·000
	1·602	0·626	0·014

Accuracy?

Table V.3. Dimensions of microphase regions.

	l_1 (μm)	l_2 (μm)	a(μm)
Widmanstätten α	0·15–0·75	0·05–0·15	
Acicular α	0·07–0·60	0·33–1·20	0·02–0·18

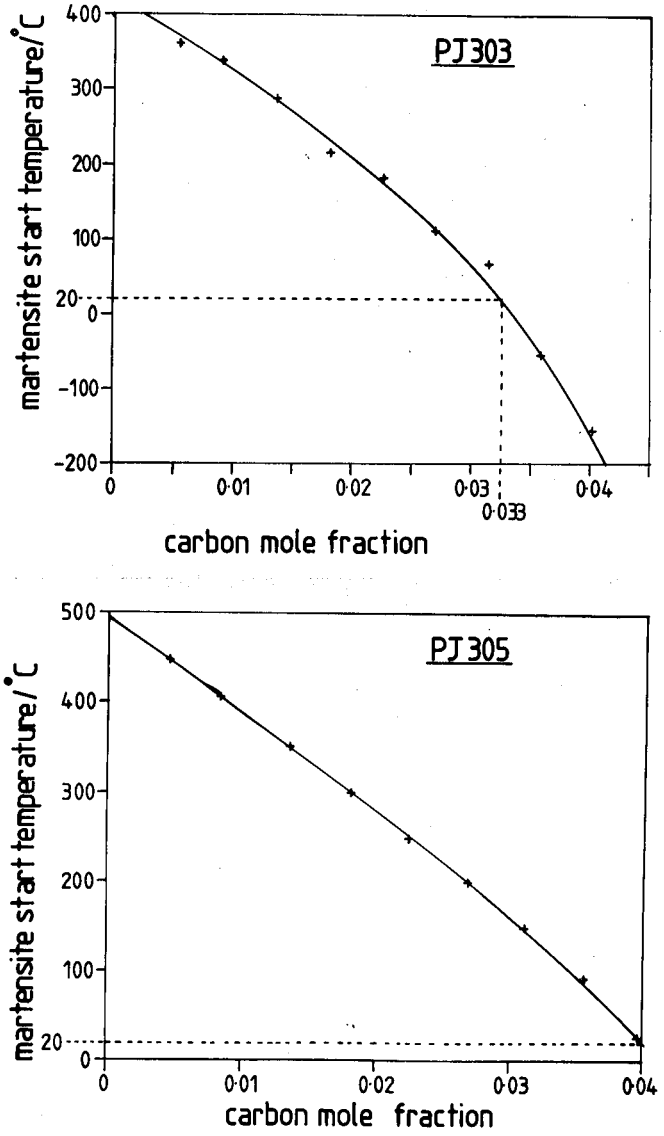

Figure 5.1. Predicted variation of M_s with carbon mole fraction in austenite.

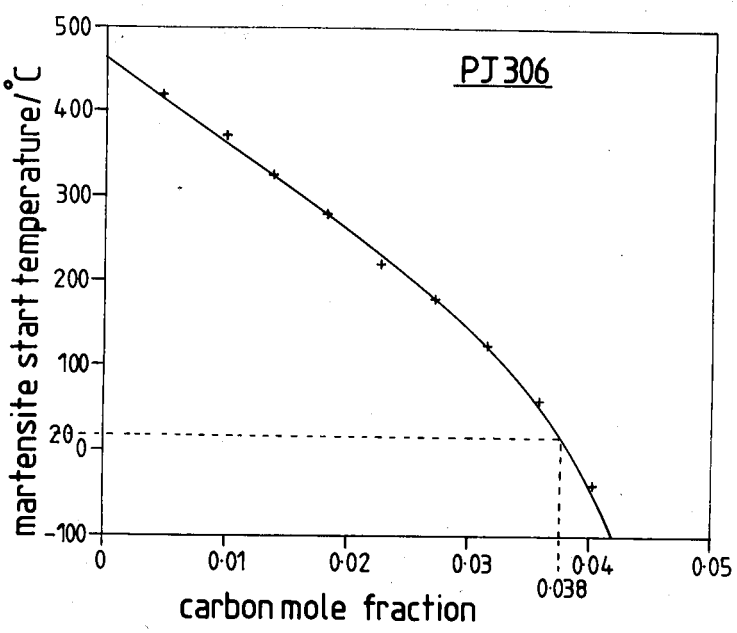

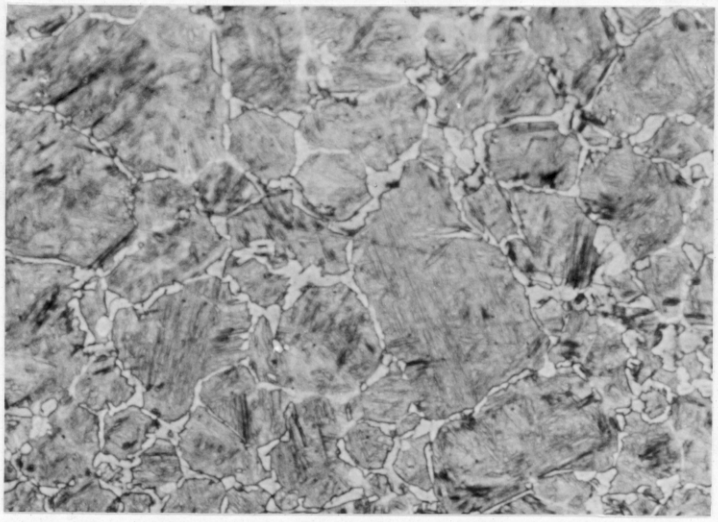

100μm

Figure 5.2. Preferential ferrite growth into one adjacent γ grain.

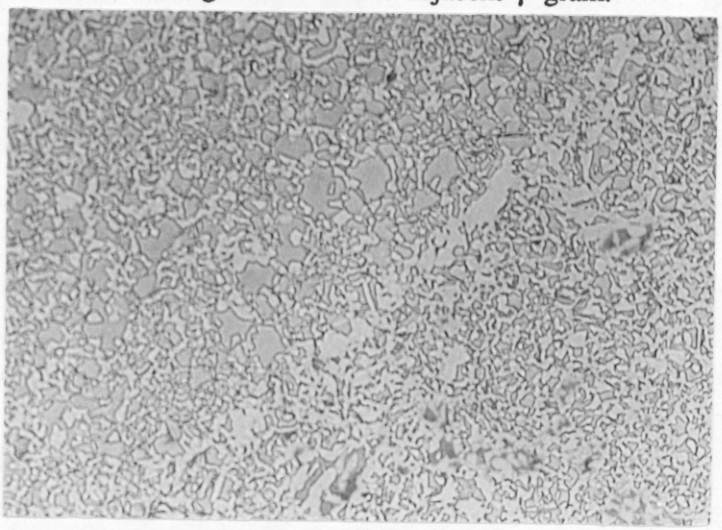

200μm

Figure 5.3. Variation in V_α throughout a specimen.

15μm

Figure 5.4. Individual bainite sheaf (centre) for small V_α.

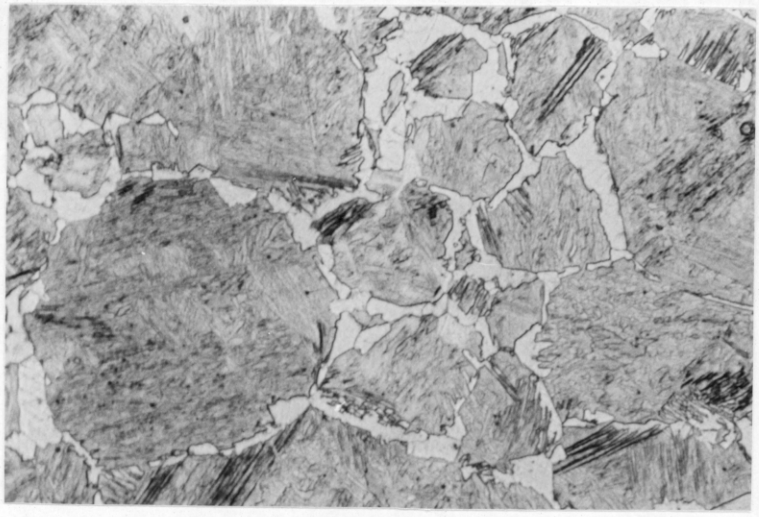

15μm

Figure 5.5. Microphase containing bainite packets.

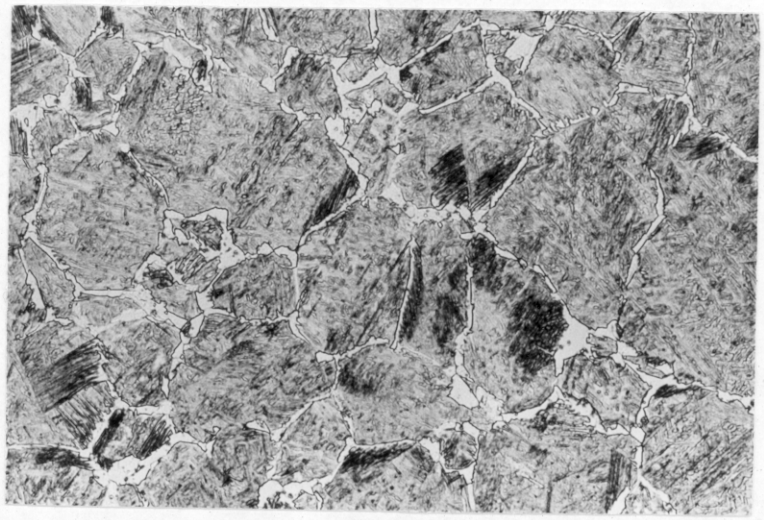

5.6(a). 40μm

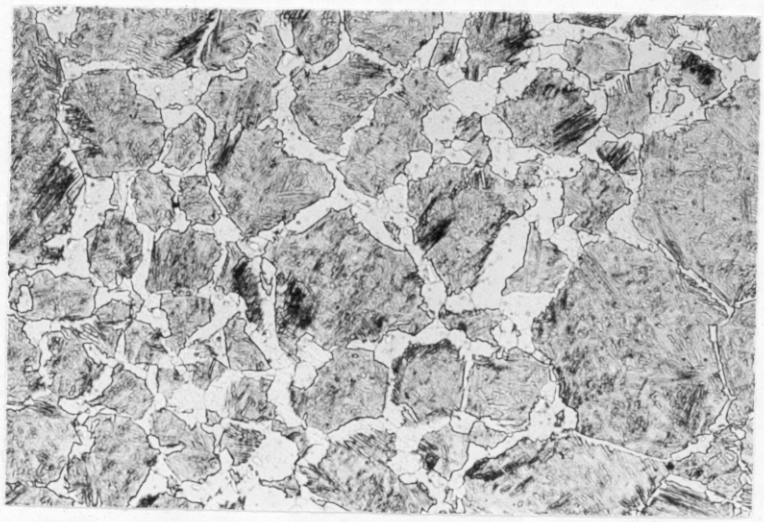

5.6(b). 40μm

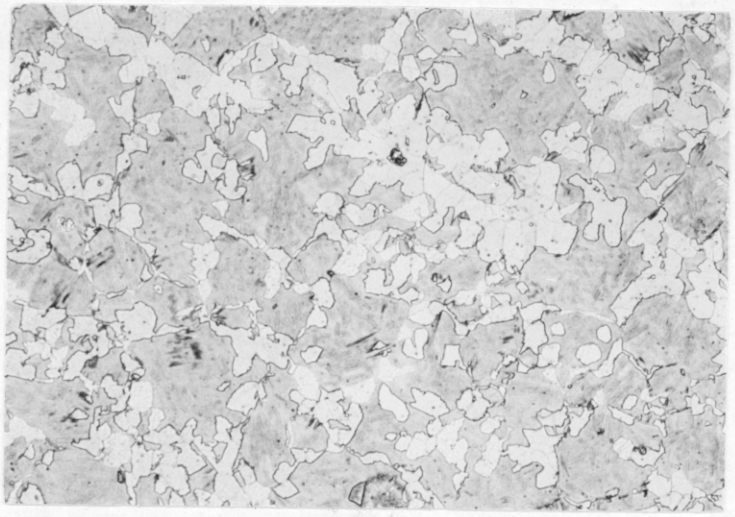

5.6(c). 40μm

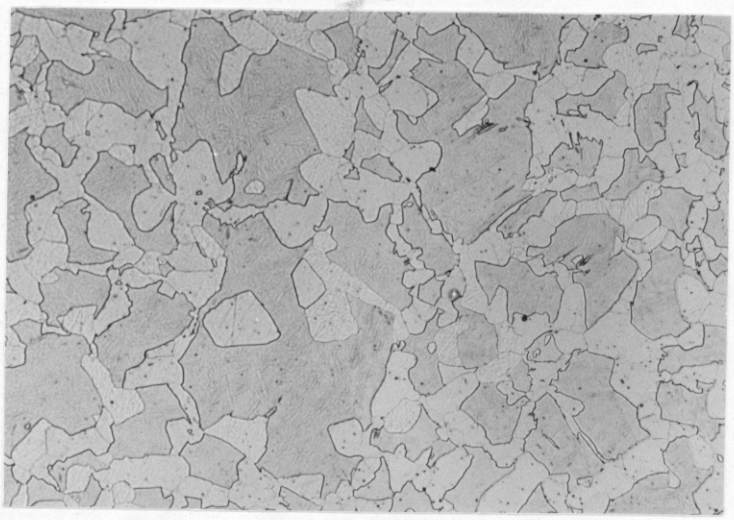

5.6(d). 40μm

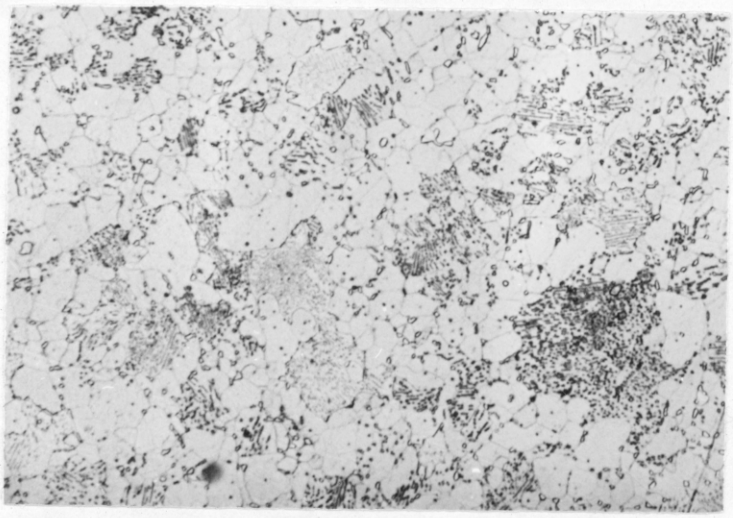

5.6(e). 40μm

Figure 5.6. Effect of increasing V_α on microphases, (a) 680°C/1800s, (b) 680°C/3600s, (c) 680°C/10800s (d) 680°C/19008s, (e) 680°C/73800s.

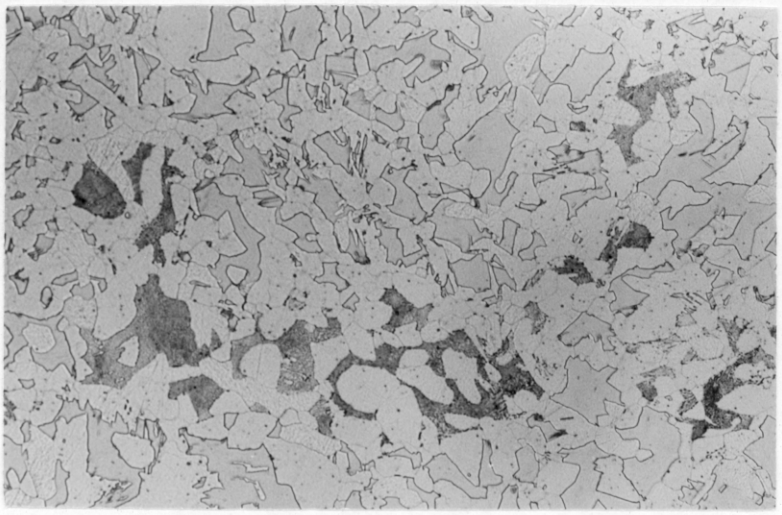

(a) 50μm

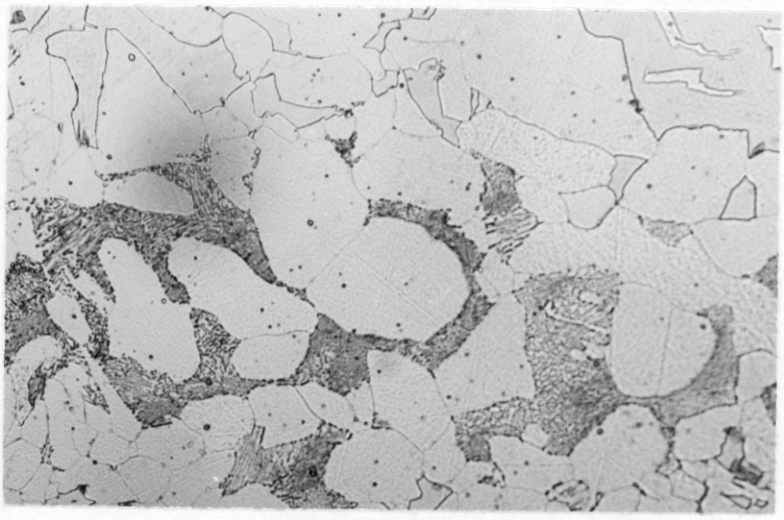

(b) 20μm

Figure 5.7. Pearlite and martensite microphase regions for PJ306 held at 680°C for 19008s. Reaustenitised at 1000°C for 10 minutes.

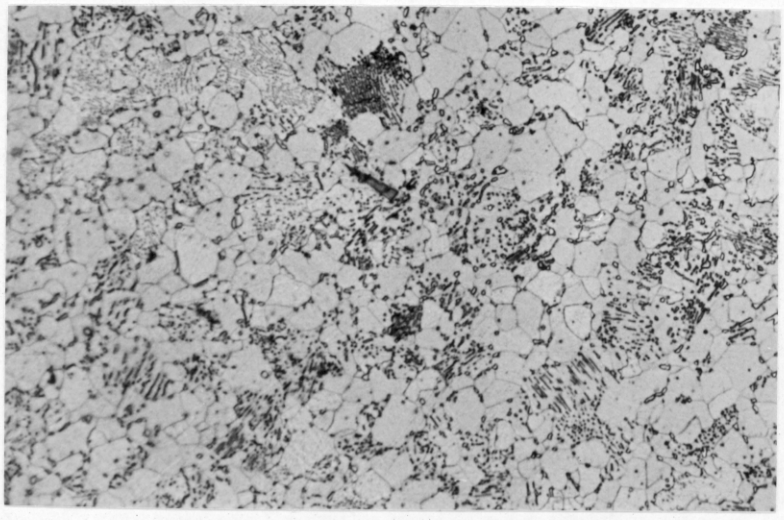

20μm

Figure 5.8. Fully pearlitic structure, PJ306, 1000°C/10 mins- 680°C/73800s.

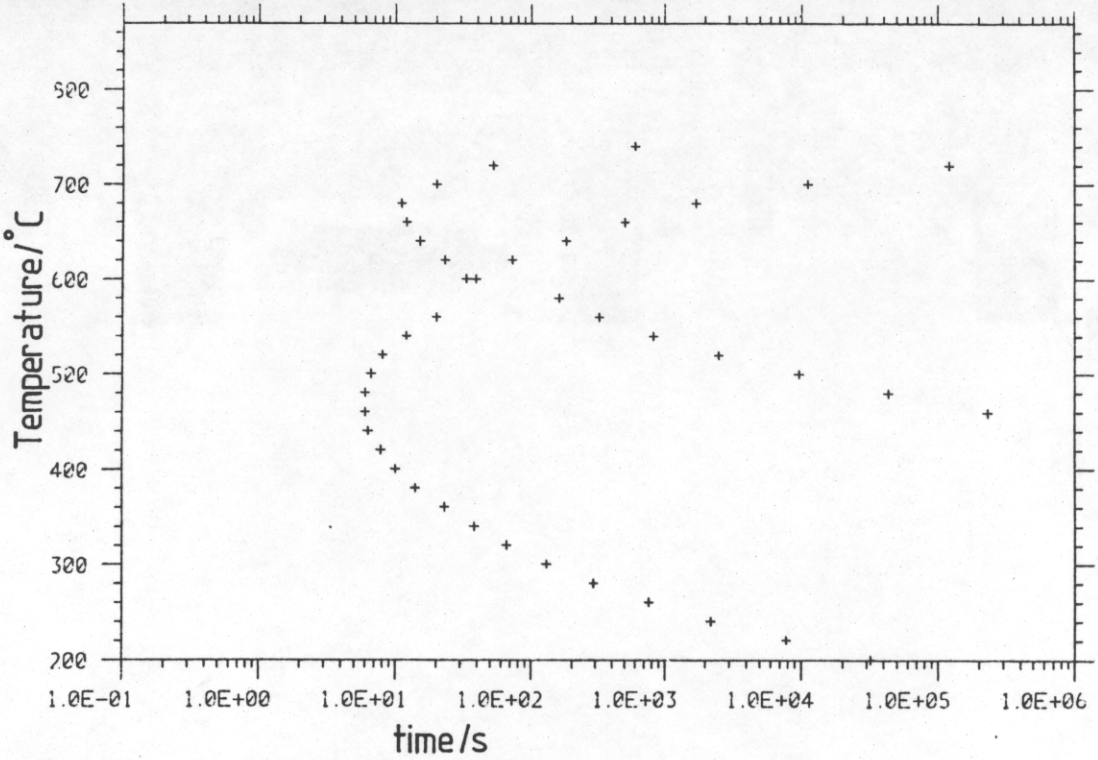

Figure 5.9. TTT curve for PJ306.

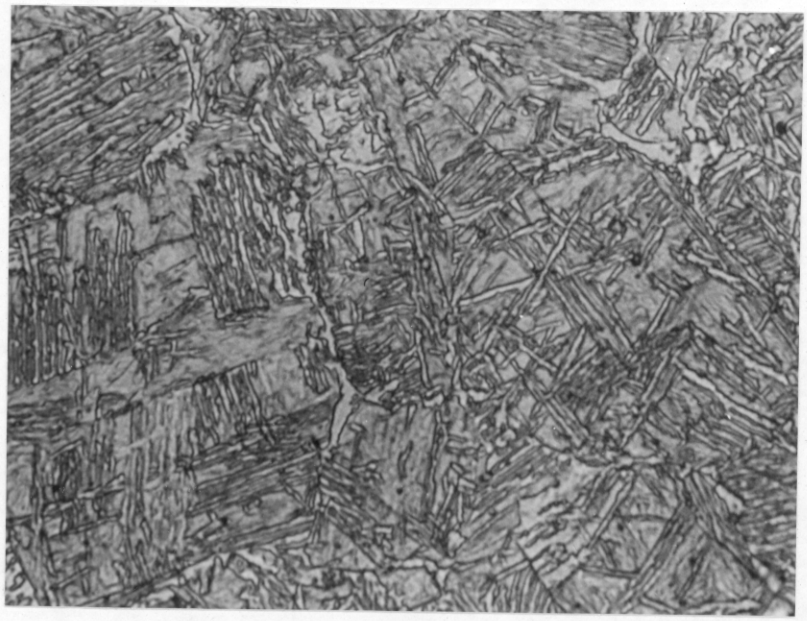

20μm

Figure 5.10. PJ305, 1000°C/10mins-500°C/5s.

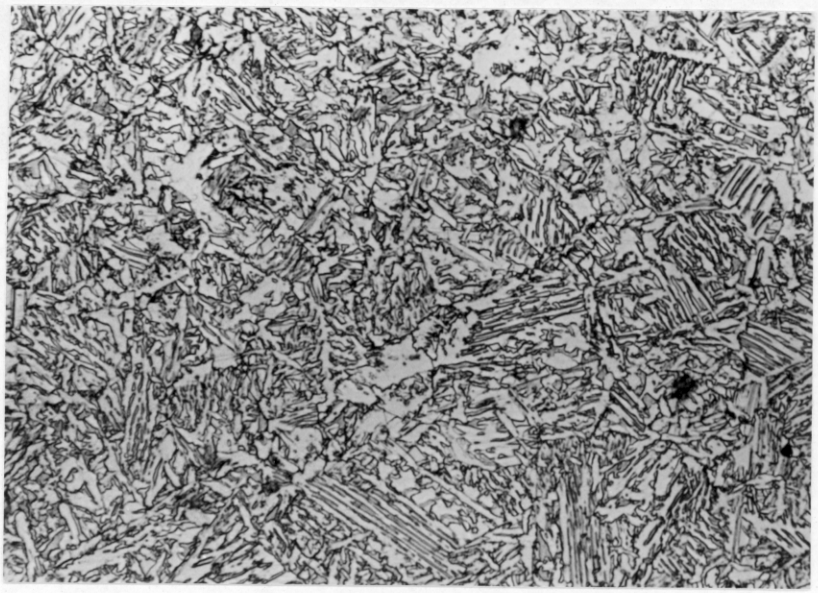

(a) 1000°C/10 mins-500°C/80s.

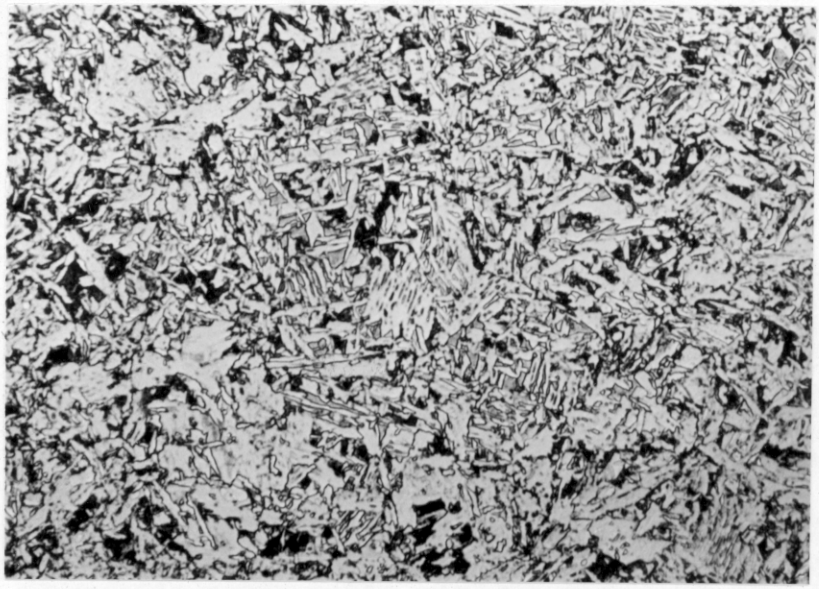

(b) 1000°C/10 mins-500°C/314s.

Figure 5.11. 20μm Increased acicularity with isothermal holding.

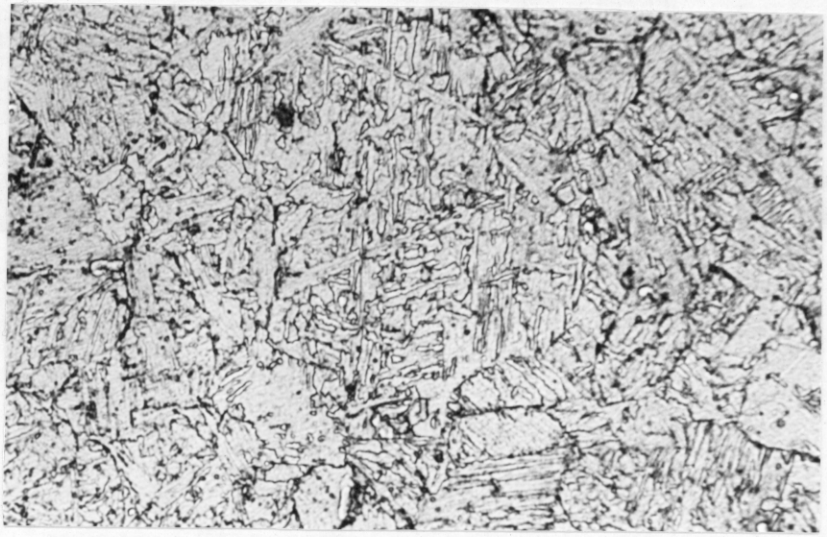

20μm

Figure 5.12. PJ305, 1000°C/10 mins-500°C/43200s.

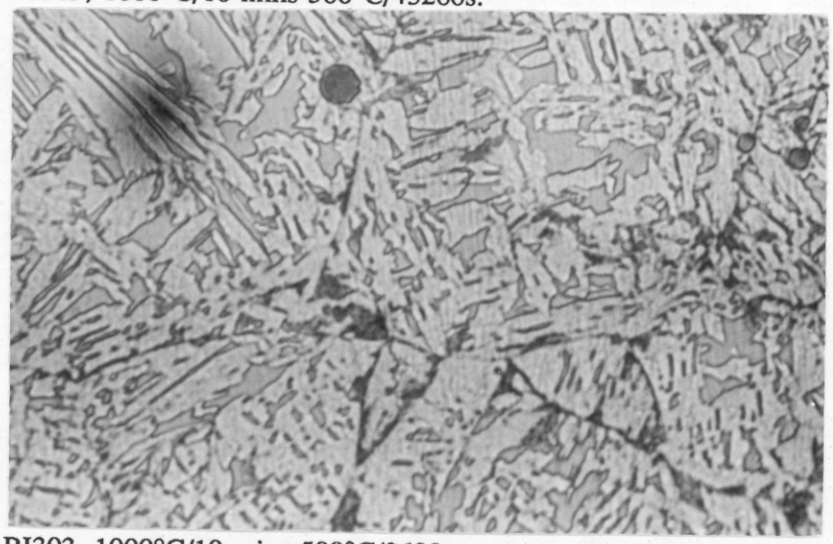

10μm

Figure 5.13. PJ303, 1000°C/10 mins-500°C/3600s.

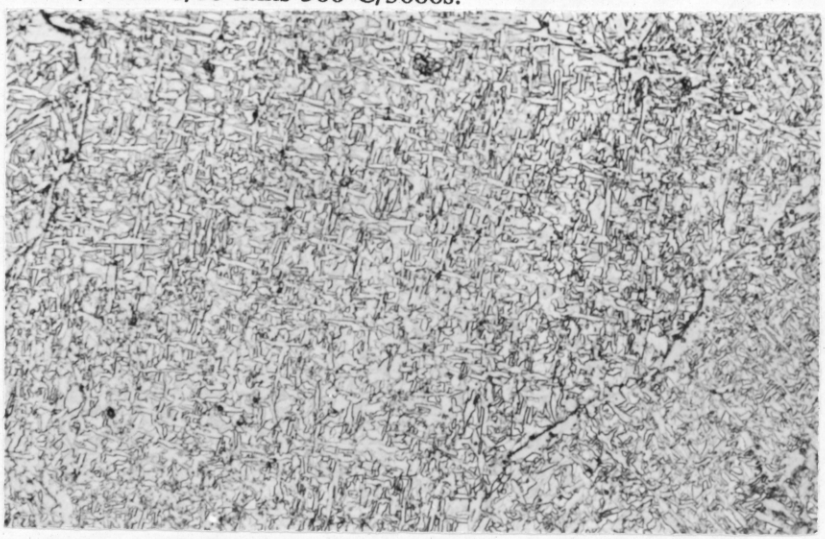

20μm

5.14(a). 1200°C/10 mins-520°C/60s.

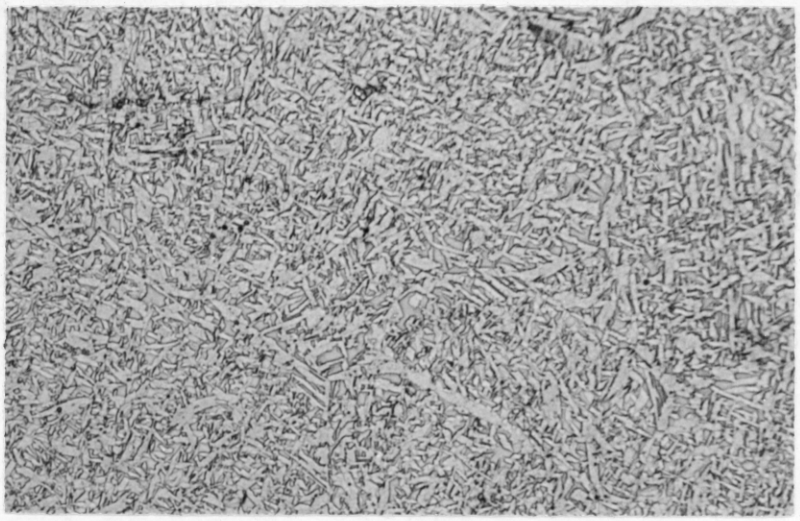

20μm

5.14(b). 1200°C/10 mins-500°C/10s.

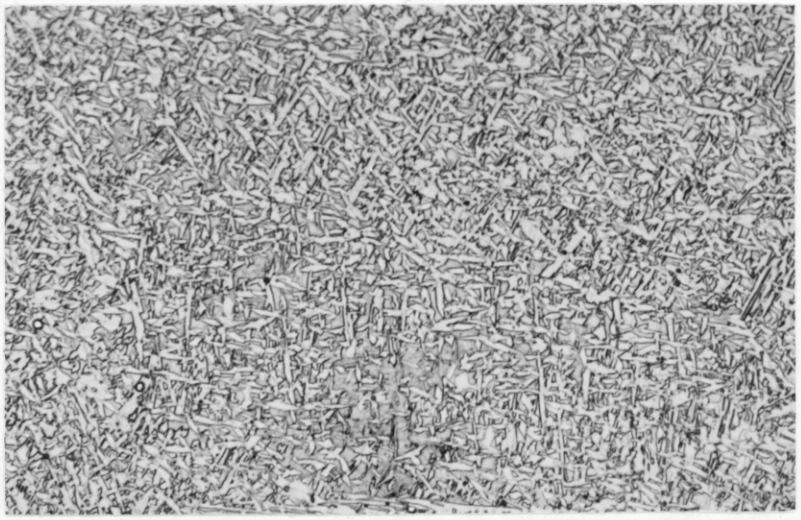

20μm

5.14(c). 1200°C/10 mins-500°C/4s.

20μm

5.14(d). 1200°C/10 mins-500°C/4s.

Figure 5.14. Microstructures after various isothermal heat treatments on PJ306 specimens.

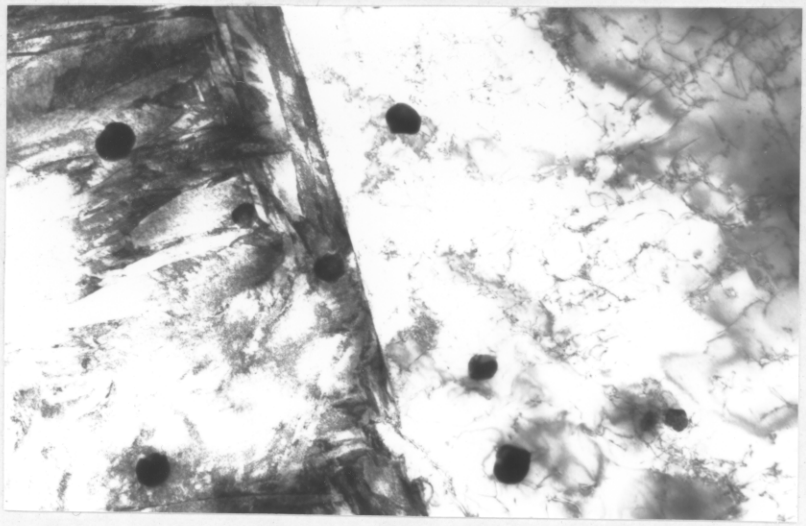

0.8μm

Figure 5.15. Allotriomorphic α and bainite microphase. PJ306, 1000°C/10 mins-680°C/1800s.

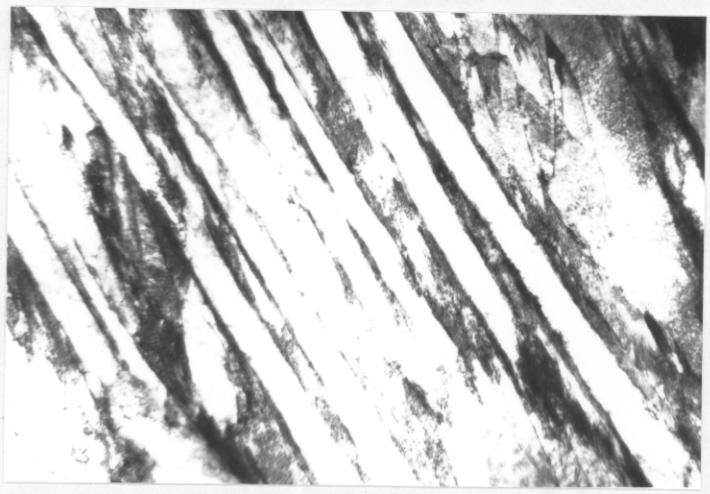

0.3μm

Figure 5.16. Highly dislocated interplate lath martensite. PJ306, 1000°C/10 mins-680°C/1800s.

0.5μm

Figure 5.17. Retained γ rimming bainite laths. PJ306, 1000°C/10 mins-680°C/1800s.

0.25μm

Figure 5.18. Autotempered martensite.

0.75μm

Figure 5.19. Allotriomorphic α, Widmanstätten α, α_b and martensite. PJ306, 1000°C/10 mins-680°C/10800s.

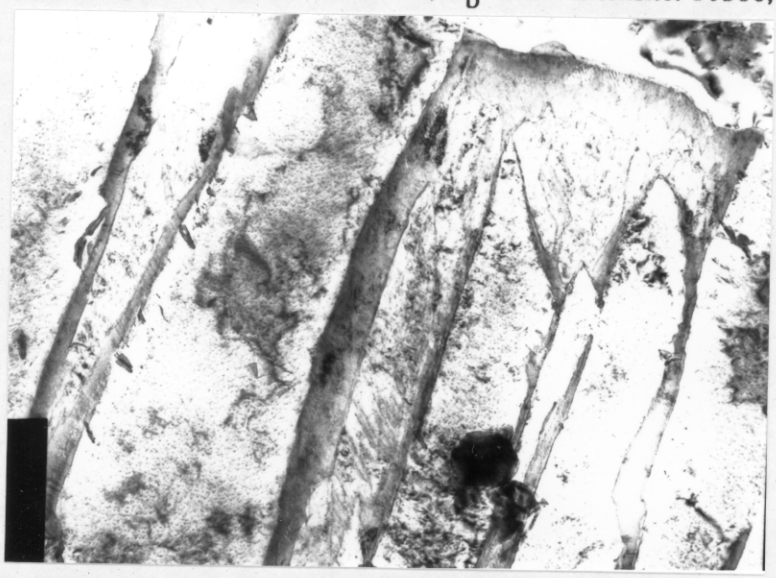

0.3μm

Figure 5.20. Striated interplate γ. PJ306, 1000°C/10 mins-680°C/10800s.

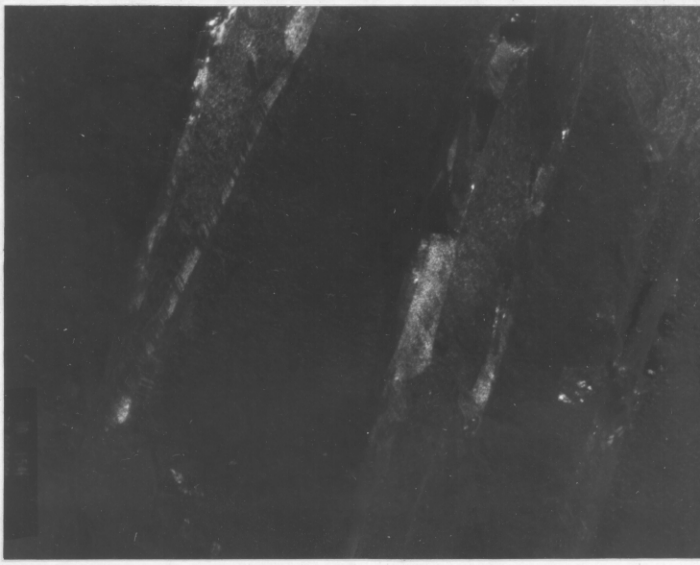

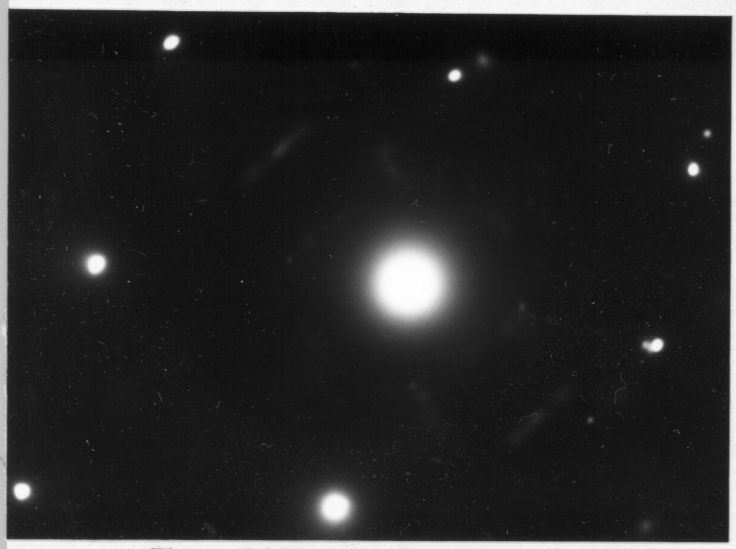

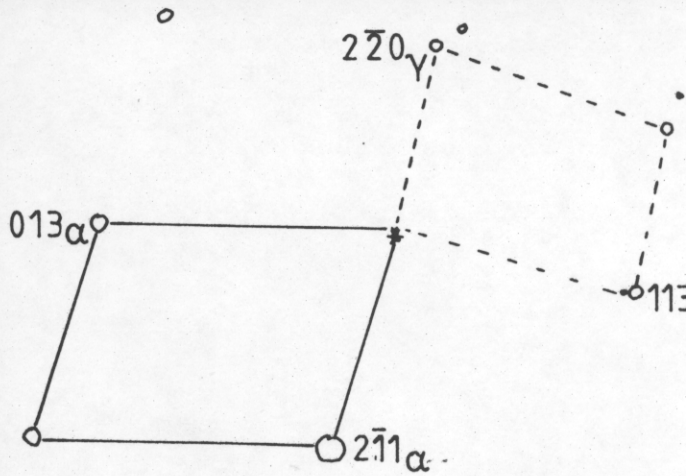

Figure 5.20(contd). Dark field and SADP.

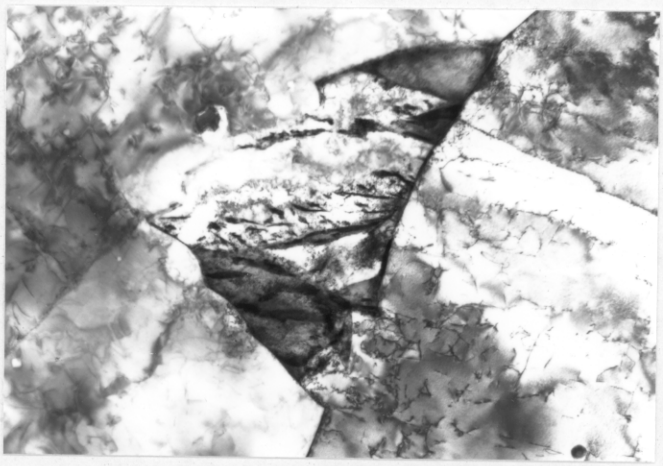

0.8μm

Figure 5.21. Formation of degenerate pearlite. PJ306, 1000°C/10 mins-680°C/10800s.

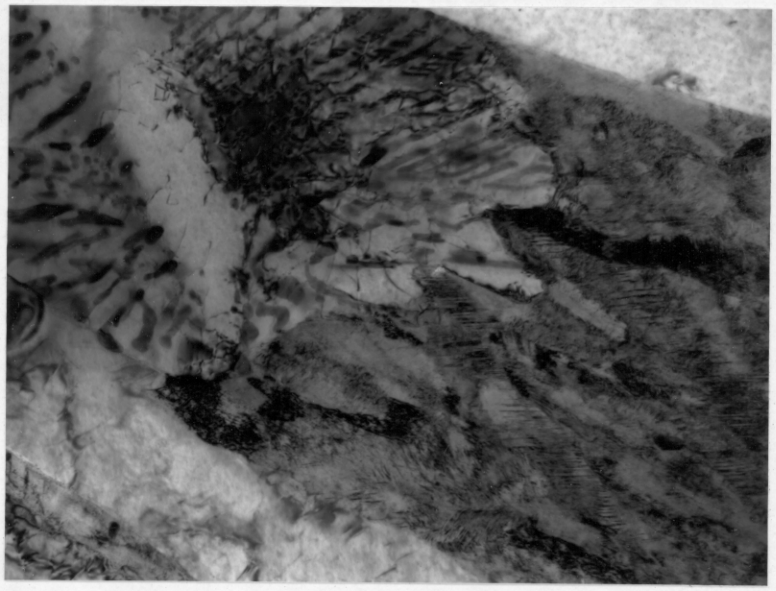

0.25μm

Figure 5.22. Formation of pearlite during isothermal treatment, leading to twinned martensite on quenching.

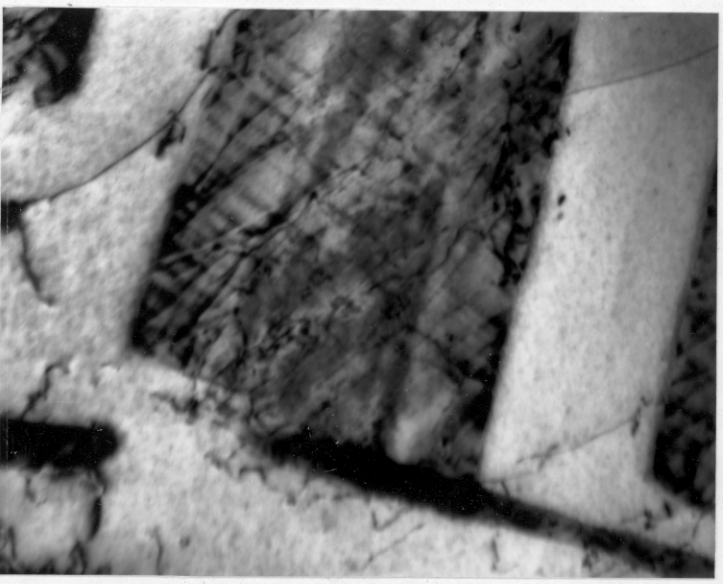

0.1μm

Figure 5.23. Dislocation cells in fully pearlitic microphase. PJ306, 1000°C/10 mins-680°C/73800s.

0.2μm

Figure 5.24. Twinned martensite between Widmanstätten α plates. PJ305, 1000°C/10 mins-500°C/80s.

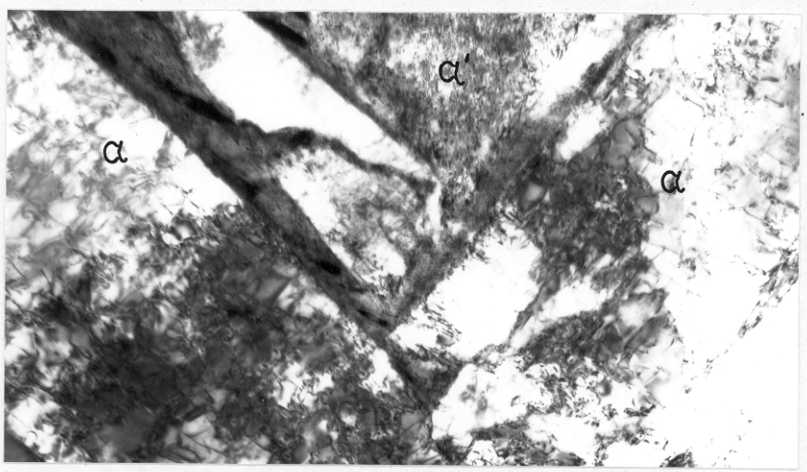

0.3μm

Figure 5.25. Thin retained γ rim between α_{acic} and lath martensite. PJ305, 1000°C/10 mins-500°C/5s.

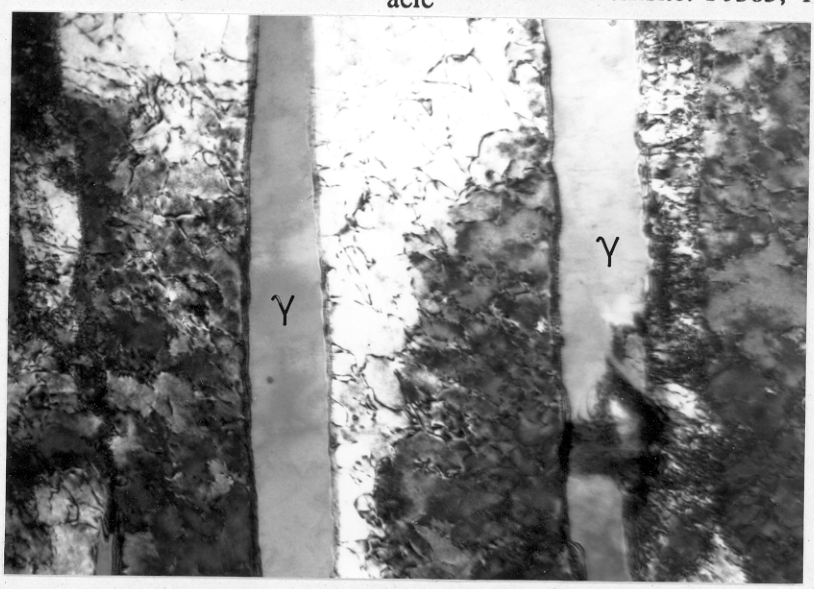

0.25μm

Figure 5.26. Retained γ between Widmanstätten α plates. PJ305, 1000°C/10 mins-500°C317s.

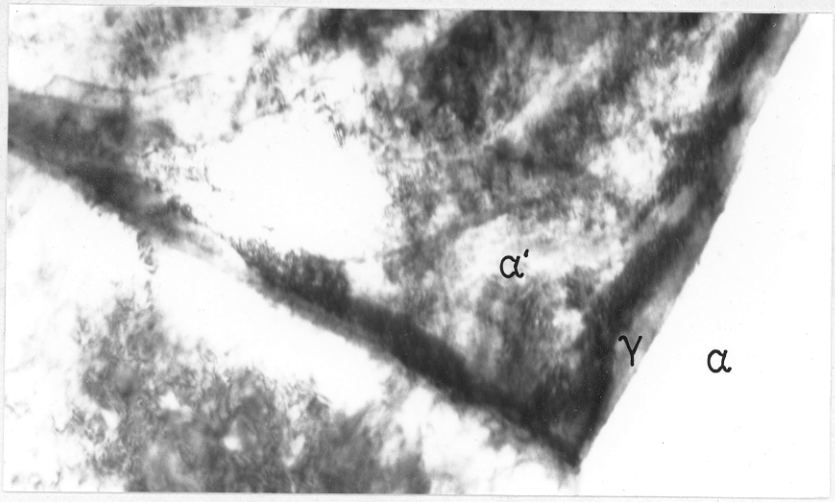

0.2μm

Figure 5.27. The formation of twinned martensite between γ_r and lath martensite in α_{acic} microphase after extended heat treatment. PJ305, 1000°C/10 mins-500°C/317s.

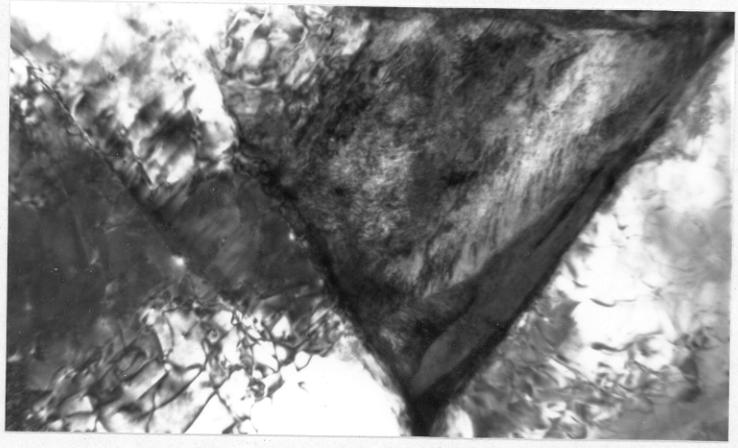

0.2μm

Figure 5.28. Lath martensite replaced by twin martensite. PJ305, 1000°C/10 mins-500°C/4068s.

0.3μm

Figure 5.29. α_{acic} microphase composed solely of twinned martensite. PJ303, 1000°C/10 mins-500°C/21100s.

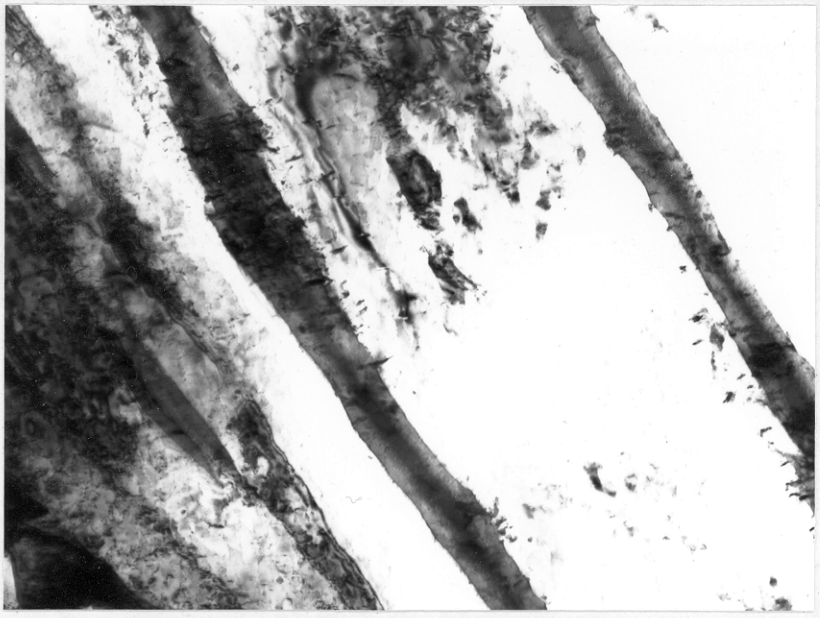

Figure 5.30. Precipitation of carbides in microphase between Widmanstätten α plates. PJ303, 1000°C/10 mins-500°C/7200s.

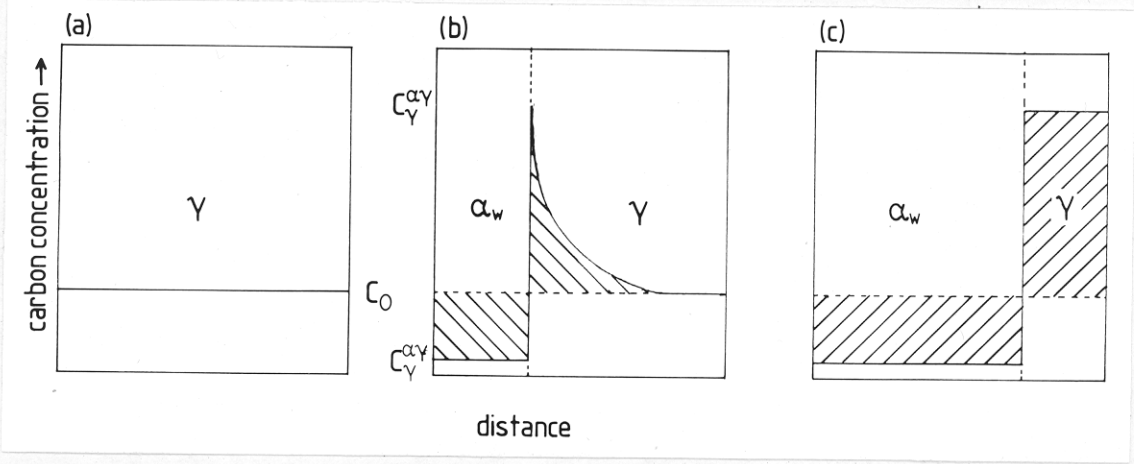

Figure 5.31. Carbon profile during and after Widmanstätten α formation.

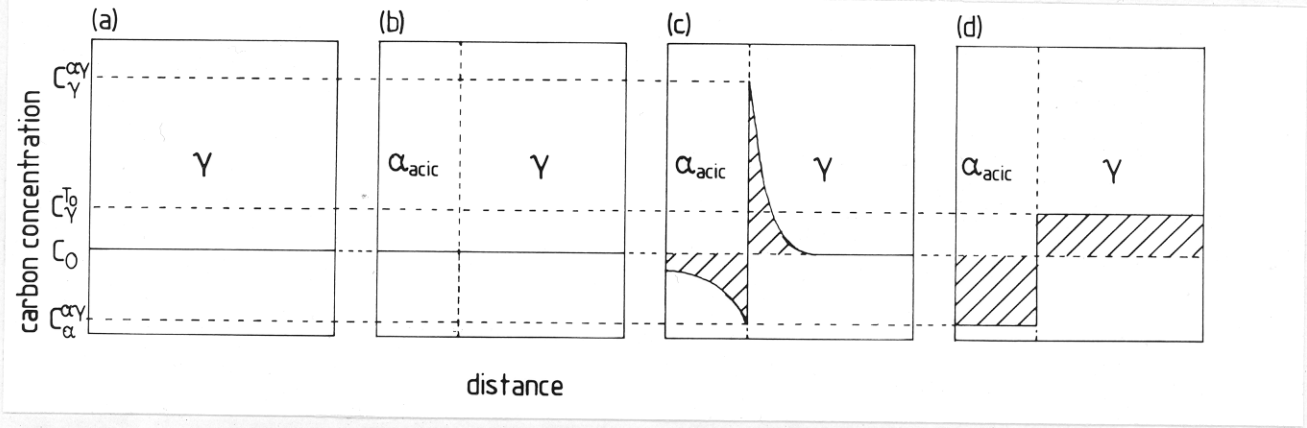

Figure 5.32. Carbon profile during and after α_{acic} formation.

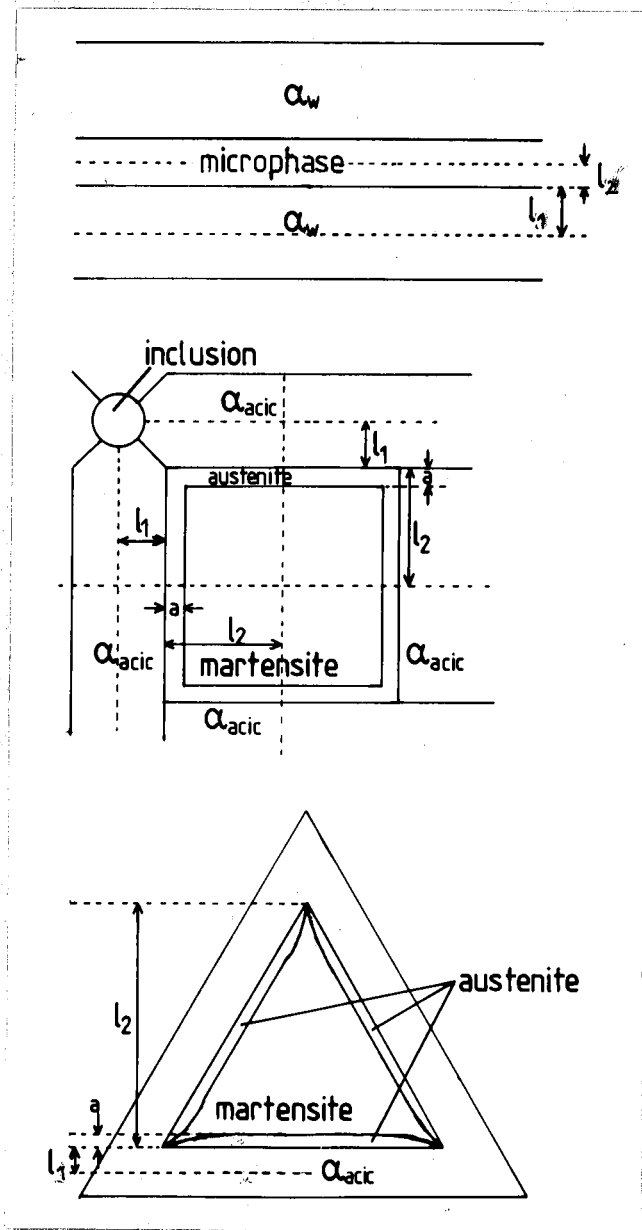

Figure 5.33. Microphase region geometries.

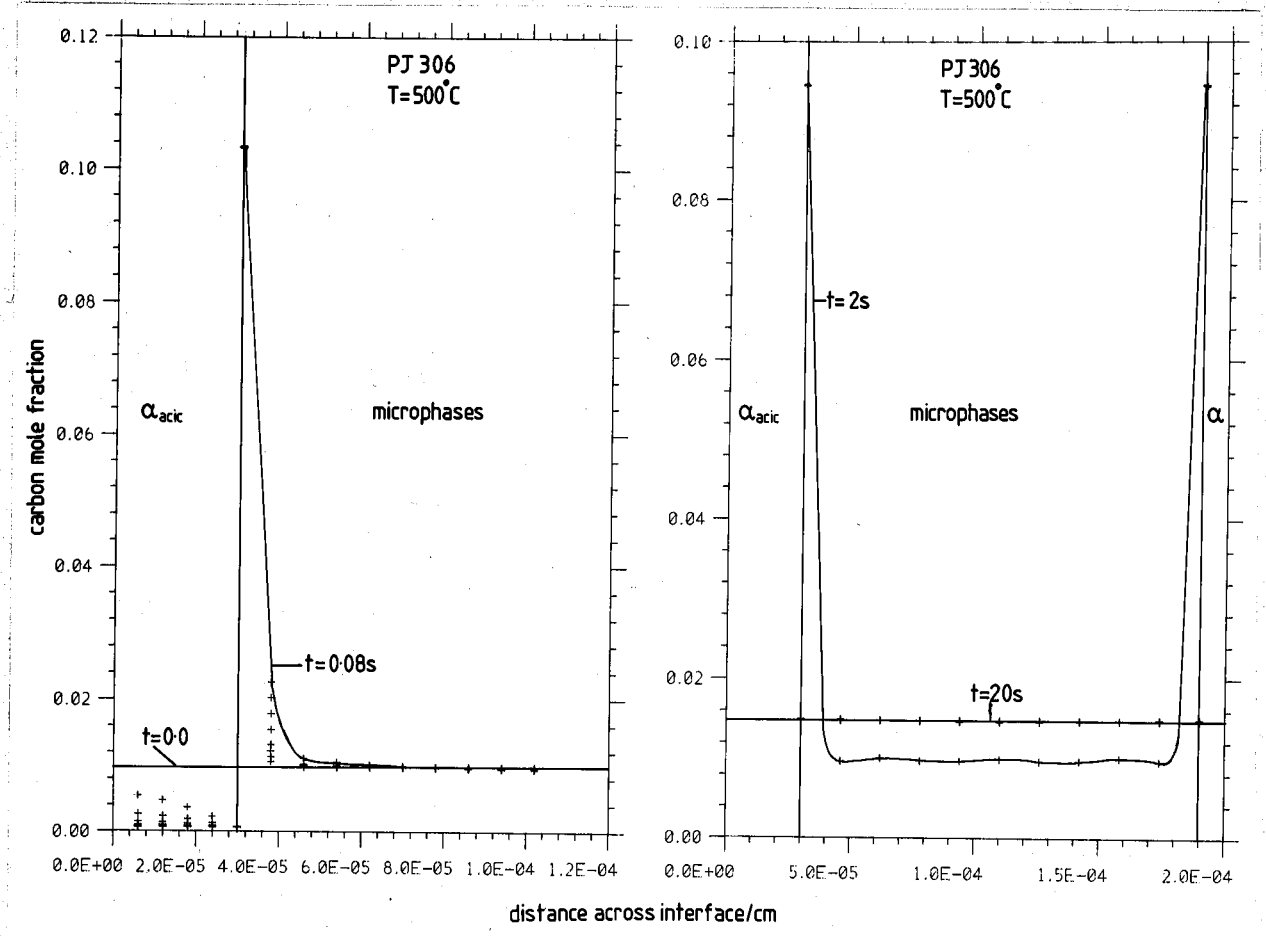

Figure 5.34. Predicted carbon profile for α_{acic} microphase regions.

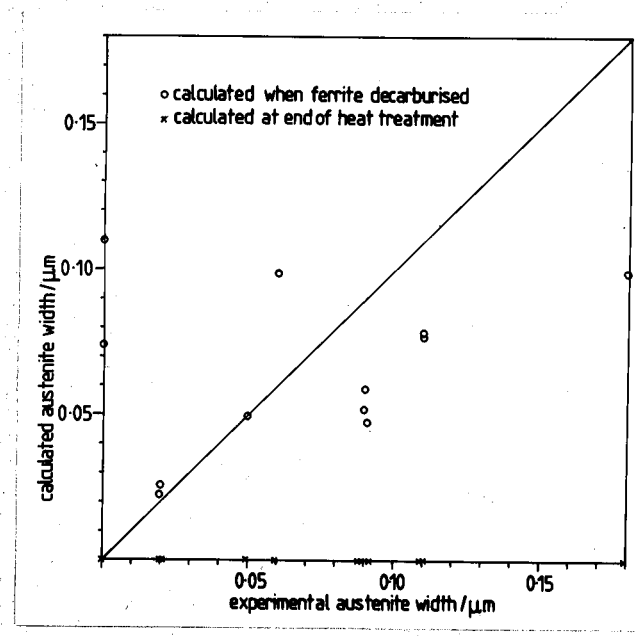

Figure 5.35. Comparison of predicted and measured γ_r

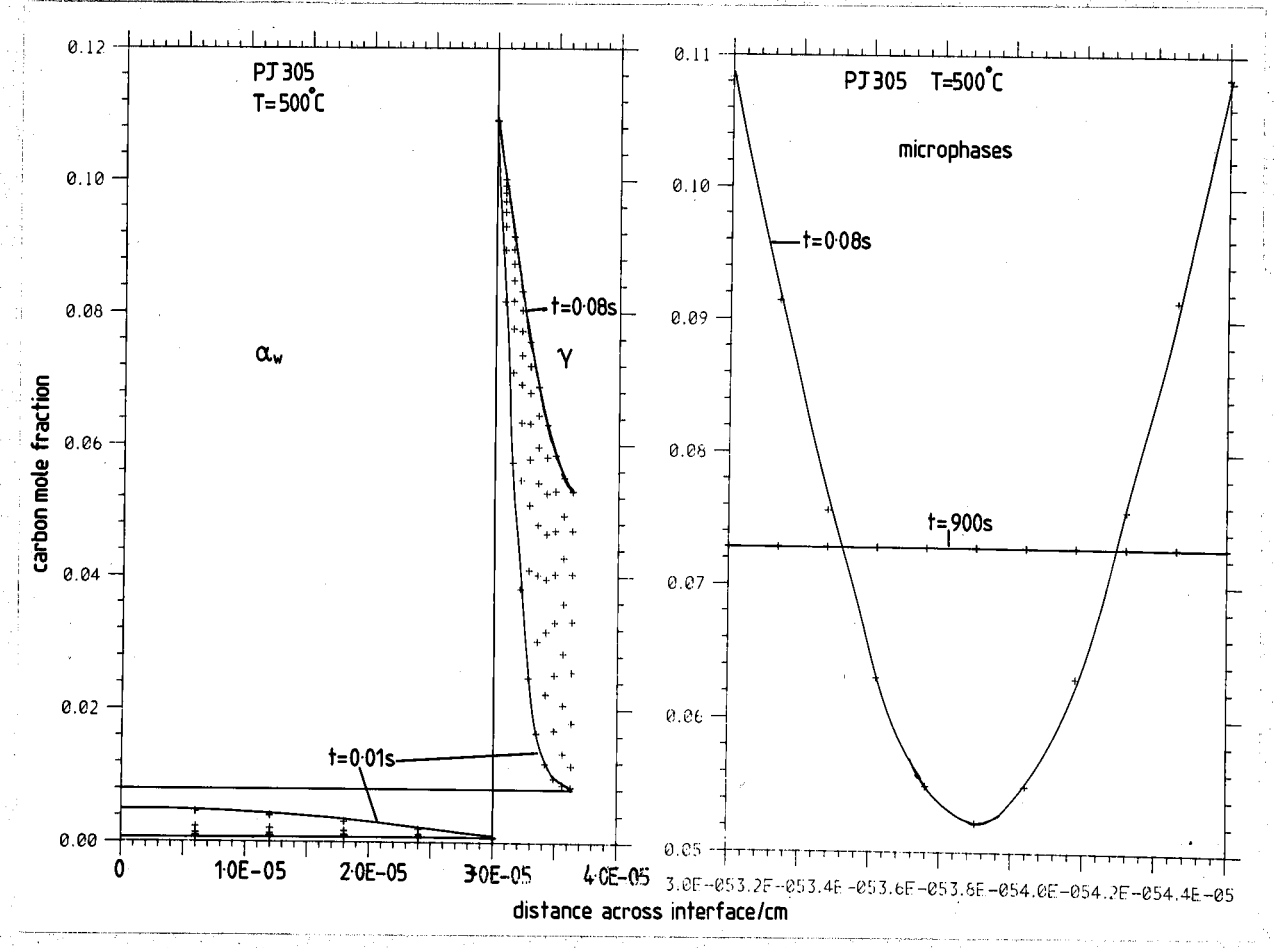

Figure 5.36. Predicted carbon profiles for Widmanstätten α microphase regions.

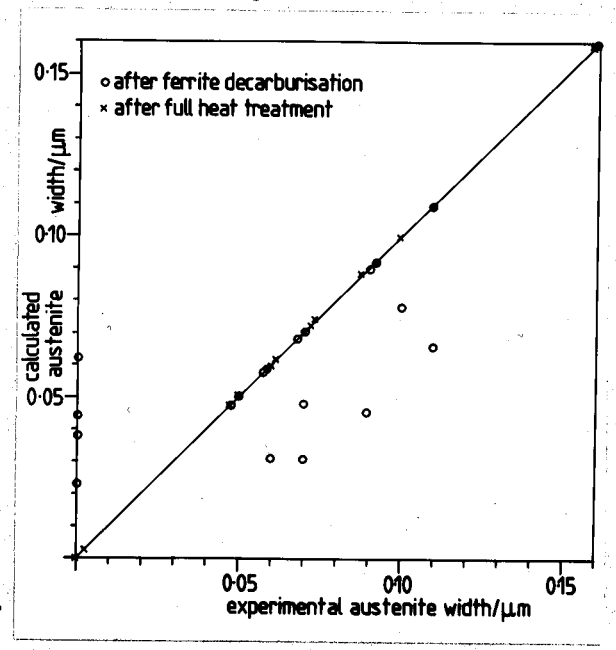

Figure 5.37. Comparison of predicted and measured γ_r

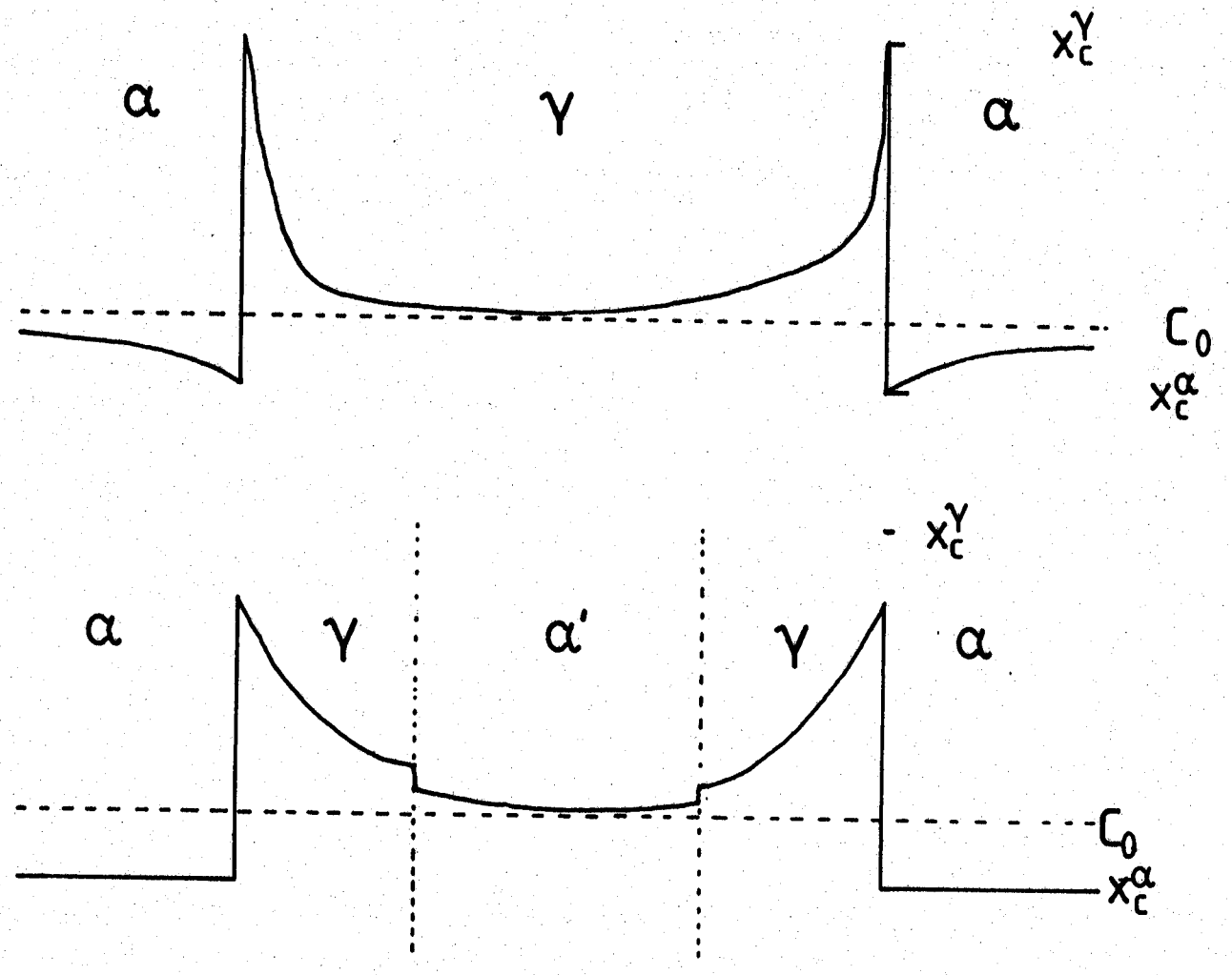

Figure 5.38. Proposed carbon profile for continuously cooled specimens.